Cellular/Molecular

NCK1 Modulates Neuronal Actin Dynamics and Promotes Dendritic Spine, Synapse, and Memory Formation

Antonios M. Diab,[1] Michael Wigerius,[1] Dylan P. Quinn,[1] Jiansong Qi,[1] Ibrahim Shahin,[1] Julia Paffile,[1] Kavita Krueger,[1] Barbara Karten,[2] Stefan R. Krueger,[3] and James P. Fawcett[1,4]

[1]Department of Pharmacology, Faculty of Medicine, Dalhousie University, Halifax, Nova Scotia B3H 4R2, Canada, [2]Department of Biochemistry and Molecular Biology, Faculty of Medicine, Dalhousie University, Halifax, Nova Scotia B3H 4R2, Canada, [3]Department of Physiology and Biophysics, Faculty of Medicine, Dalhousie University, Halifax, Nova Scotia B3H 4R2, Canada, and [4]Department of Surgery, Faculty of Medicine, Dalhousie University, Halifax, Nova Scotia B3H 4R2, Canada

Memory formation and maintenance is a dynamic process involving the modulation of the actin cytoskeleton at synapses. Understanding the signaling pathways that contribute to actin modulation is important for our understanding of synapse formation and function, as well as learning and memory. Here, we focused on the importance of the actin regulator, noncatalytic region of tyrosine kinase adaptor protein 1 (NCK1), in hippocampal dependent behaviors and development. We report that male mice lacking NCK1 have impairments in both short-term and working memory, as well as spatial learning. Additionally, we report sex differences in memory impairment showing that female mice deficient in NCK1 fail at reversal learning in a spatial learning task. We find that NCK1 is expressed in postmitotic neurons but is dispensable for neuronal proliferation and migration in the developing hippocampus. Morphologically, NCK1 is not necessary for overall neuronal dendrite development. However, neurons lacking NCK1 have lower dendritic spine and synapse densities *in vitro* and *in vivo*. EM analysis reveal increased postsynaptic density (PSD) thickness in the hippocampal CA1 region of NCK1-deficient mice. Mechanistically, we find the turnover of actin-filaments in dendritic spines is accelerated in neurons that lack NCK1. Together, these findings suggest that NCK1 contributes to hippocampal-dependent memory by stabilizing actin dynamics and dendritic spine formation.

Key words: actin; memory; NCK; synapse

Significance Statement

Understanding the molecular signaling pathways that contribute to memory formation, maintenance, and elimination will lead to a better understanding of the genetic influences on cognition and cognitive disorders and will direct future therapeutics. Here, we report that the noncatalytic region of tyrosine kinase adaptor protein 1 (NCK1) adaptor protein modulates actin-filament turnover in hippocampal dendritic spines. Mice lacking NCK1 show sex-dependent deficits in hippocampal memory formation tasks, have altered postsynaptic densities, and reduced synaptic density. Together, our work implicates NCK1 in the regulation of actin cytoskeleton dynamics and normal synapse development which is essential for memory formation.

Introduction

Memory formation and maintenance is a dynamic process that can be modulated by changes in receptor function and structural changes at synapses through the remodeling, enlargement, elimination, and/or addition of synaptic connections (Caroni et al., 2012; Bailey et al., 2015; Basu and Lamprecht, 2018). The actin cytoskeleton plays a critical role in modulating structural changes that are associated with memory formation. Indeed, interfering with actin rearrangement by pharmacologically blocking actin polymerization during or directly after learning impairs memory formation (Mantzur et al., 2009; Rehberg et al., 2010; Nelson et al., 2012).

The majority of excitatory synapses in the brain occur on specialized actin-rich protrusions on dendrites, known as dendritic

Received Mar. 8, 2021; revised Dec. 5, 2022; accepted Dec. 10, 2022.

Author contributions: A.M.D., M.W., D.P.Q., B.K., S.R.K., and J.P.F. designed research; A.M.D., M.W., D.P.Q., J.Q., I.S., J.P., K.K., S.R.K., and J.F. performed research; K.K. and B.K. contributed unpublished reagents/analytic tools; A.M.D., J.Q., I.S., J.P., and J.P.F. analyzed data; A.M.D. wrote the first draft of the paper; A.M.D., M.W., D.P.Q., B.K., S.R.K., and J.P.F. edited the paper; A.M.D. and J.P.F. wrote the paper.

This work was supported by Canadian Institutes of Health Research Grants MOP-84366, 79413, and PJT-159738 (to J.P.F.) and Natural Sciences and Engineering Research Council of Canada Discovery Grants RGPIN/005562-2018 and RGPIN 326821 (to B.K. and S.R.K.). We thank Mary Ann Trevors, facility manager of the electron microscope facility at Dalhousie University, for technical support and specimen preparation for the transmission electron microscope.

The authors declare no competing financial interests.

Correspondence should be addressed to James P. Fawcett at jim.fawcett@dal.ca.

https://doi.org/10.1523/JNEUROSCI.0495-21.2022

spines, that function to compartmentalize and control signaling cascades important for neuronal communication. Memory formation is associated with changes in dendritic spine morphology, stability, and number (Lamprecht and LeDoux, 2004; Yang et al., 2009; Bailey et al., 2015). Learning alters dendritic spine density in brain circuits that are recruited during task performance (Xu et al., 2009; Wang et al., 2011), and motor task learning can be disrupted experimentally by optical shrinkage of task potentiated spines (Hayashi-Takagi et al., 2015). In addition, abnormal dendritic spine plasticity, morphology, and number are associated with learning impairments (Sala and Segal, 2014; Chazeau and Giannone, 2016). Finally, memory and learning deficits are associated with abnormal dendritic spine numbers in several neurologic disorders (Fiala et al., 2002; Herms and Dorostkar, 2016; Martínez-Cerdeño, 2017).

Dendritic spines contain a protein-dense region known as the postsynaptic density (PSD) which clusters neurotransmitter receptors and initiates biochemical changes in the postsynaptic neuron. In response to neuronal stimulation, the PSD becomes thicker, suggesting that activity-dependent recruitment of proteins occurs in this region (Dosemeci et al., 2001). The PSD undergoes actin-dependent remodeling (Blanpied et al., 2008; Minerbi et al., 2009) that has been linked to learning and memory formation (Fonseca et al., 2006; Karpova et al., 2006; Nagura et al., 2012). Despite recent evidence outlining activity-induced regulation of the PSD, it remains unclear which proteins and signaling pathways are involved.

Actin-regulatory proteins have been shown to play a critical role in learning and memory formation (Grove et al., 2004; Soderling et al., 2007; Haditsch et al., 2009; Rust et al., 2010). Modulation of the actin cytoskeleton is controlled by small GTPases, such as Rac1, Cdc42, RhoA, and their downstream effectors including PAK, N-WASP, WAVE, and Arp2/3 (Chazeau and Giannone, 2016). Together with glutamate, Eph receptors, and adhesion molecules, these actin regulators play fundamental roles in spine morphogenesis and memory formation (Woolfrey and Srivastava, 2016). However, the molecular details that define these signaling complexes remain elusive.

In vitro studies have linked the noncatalytic region of tyrosine kinase adaptor protein (NCK) family of adaptor proteins, which consists of two members, NCK1 and NCK2, with actin regulators, including PAK, N-WASP, and Arp2/3 (Bokoch et al., 1996; Zhao et al., 2000; Cowan and Henkemeyer, 2001; Rohatgi et al., 2001; Thévenot et al., 2011), and with cell surface receptors, including Eph receptors, ephrin family members, and DCC (Holland et al., 1997; Zhao et al., 2000; Cowan and Henkemeyer, 2001; Rohatgi et al., 2001; Li et al., 2002; Thévenot et al., 2011), that have been implicated in memory and learning (Meng et al., 2005; Kelly and Chernoff, 2012; Horn et al., 2013; Kim et al., 2013; Dines and Lamprecht, 2015; Civiero and Greggio, 2018), suggesting that the NCK family of proteins may function to link synaptic receptor signaling events to actin dynamics during memory formation and learning.

NCK1 and NCK2 are 47-kDa proteins that consist of four protein-binding domains, one SH2 domain and three SH3 domains. They share 68% amino-acid identity, which rises to 80–85% identity when comparing their protein binding domains only (Chen et al., 1998). Both NCK proteins are expressed in a wide variety of tissues and are considered functionally redundant during development. Loss of both NCK1 and NCK2 results in embryonic lethality, whereas mice deficient for either protein are viable (Bladt et al., 2003; Fawcett et al., 2007). However, it has not been determined whether NCK1 and NCK2 are functionally redundant in the adult brain and although *in vitro* studies have shown that NCK1 is localized to dendrites and enriched in dendritic spines and protrusions (Pilpel and Segal, 2005), it remains uncertain whether NCK1 plays a role in memory and learning.

Here, we used mice lacking NCK1 ($NCK1^{-/-}$) to determine whether this protein is important for memory and/or learning. We report that male $NCK1^{-/-}$ mice have impairments in short-term social recognition, in working memory, and in spatial learning as assessed in the Morris water maze test, while female $NCK1^{-/-}$ mice fail at reversal learning in the Morris water maze test. Further analysis of the hippocampus revealed that NCK1 is expressed exclusively in postmitotic neurons and is not necessary for neuronal proliferation, migration, or patterning. However, NCK1 deficiency results in decreased dendritic spine density and increased PSD thickness. Mechanistically, we show that loss of NCK1 alters actin-filament dynamics in dendritic spines. Our data uncover a novel role for NCK1 in dendritic spines that link to the associated defects in hippocampal-based memory and learning in $NCK1^{-/-}$ mice.

Materials and Methods

Animals

NCK1 mutant mice and their control littermates were bred in-house on a ICR and C57BL/6 mixed genetic background (Bladt et al., 2003). Two- to four-month-old adult mice were used for all experiments unless otherwise stated. For time-pregnancy experiments, embryonic day (E) was defined from vaginal plug detection as E0.5. Rooms were maintained at 21°C under a 12/12 h light/dark cycle (7 A.M. to 7 P.M. lights on). Food and water were available *ad libitum*. The study was approved by the Dalhousie University Committee on Laboratory Animals (Dalhousie Animal Protocol #14-062) and was conducted according to the Canadian Council on Animal Care guidelines.

Behavioral testing

Social interaction/social recognition test

Modified from (Moy et al., 2004), briefly, male and female mice were placed into the middle chamber of a three-chambered apparatus and after a 2-min acclimatization period, mice were allowed to freely explore the three chambers. During the social interaction trial one chamber contained a caged mouse (of the same sex and age from a different litter), and the opposite chamber contained an empty cage. The time the subject mouse spent interacting (sniffing/touching) with each cage was recorded over 5 min. The social recognition trial was a 5-min trial run an hour later. The subject mouse was presented with the mouse that was previously present during the social interaction trial (familiar) in one cage, and with an unfamiliar mouse of the same age and sex from a different litter in the second cage. The time spent interacting with each cage was recorded.

Spontaneous alternations in a Y-maze

Adapted from (Lalonde, 2002), briefly, the subject mouse is placed in the center of a symmetrical Y-maze and allowed to run freely for 5 min and each arm entry is recorded. Alternations are scored as overlapping triplet sets in which three different arms are entered (e.g., ABC, BCA, CAB, BAC, etc.). A percent alternation score is determined by (number of alternations/(total number of arm entries – 2)) × 100.

Morris water maze

Testing protocol was adapted from (A.A. Wong and Brown, 2007), briefly, mice were tested in a 115-cm diameter water filled pool (room temperature) made opaque by the addition of nontoxic white liquid tempera paint (Schola). The escape platform consisted of a clear Plexiglas cylinder (10-cm diameter). Mice were tested four trials/day for eight consecutive days, followed by a single probe trial on day 9, and an additional four trials on day 10 using a visible platform. Trials timed out when the mouse mounted the escape platform or at 60 s if the mice did not escape, in which case mice were led to the escape platform and left

on it for 30 s. For each trial, mice were released into the pool at a different randomly assigned start position (North, South, East, West). Testing occurred in four phases: acquisition, reversal, probe, and visible platform trials. During acquisition (days 1–4), the platform was hidden in the northwest quadrant. During reversal (days 5–8), the platform was hidden in the southeast quadrant. During the probe trial (day 9), there was no platform, mice were released from the South start position, and were left in the pool for the complete 60 s. During the visible platform trials (day 10), a visible platform was placed in the northeast quadrant. Swim paths were recorded using a video camera-based tracking system and WatermazeBeta software (Actimetrics). Swim paths and percentage of time spent in each quadrant were recorded and analyzed.

Adult mouse brain histology

Male mice were deeply anesthetized (sodium pentobarbital, 2.4 mg/g i.p.; Bimeda-MTC Animal Health Inc.), perfused transcardially with PBS followed by 4% paraformaldehyde (PFA). Brains were dissected, fixed (4% PFA, 5 h), washed (PBS 3 × 20 min), cryoprotected (30% sucrose, 48 h at 4°C), embedded (Tissue Tek), and sectioned.

Free-floating sections were washed in a solution of 0.25% Triton X-100 in PBS (t-PBS) 3 × 10 min, transferred to 1% Triton X-100 in PBS for 10 min, blocked in 10% normal goat serum (NGS) t-PBS for 1 h, incubated in primary antibody solution containing 3% NGS in t-PBS overnight at 4°C. The primary antibodies used in this study include chicken anti-β-Galactosidase (1:1000; Abcam, ab9361), mouse anti-NeuN (Millipore, MAB377), rabbit anti-Iba1 (Wako Chemicals, 019-19741, 1:1000), Sox2 (Santa Cruz Biotechnology, sc-17320, 1:1000). Following overnight incubation in primary antibody, sections were washed 3 × 10 min in t-PBS and incubated with the following secondary antibodies, Alexa Fluor 488 goat anti-chicken (1:500, Lie Technologies, A11039), Alexa Fluor 594 goat anti-mouse (1:500, Invitrogen, A11005), Alexa Fluor 647 goat anti-rabbit (1:500, Life Technologies, A21246), Alexa Fluor 594 goat anti-rabbit (1:500, Invitrogen, A11037), Alexa Fluor 488 goat anti-mouse (1:500, Invitrogen, A11029). Following incubation, sections were washed, incubated in Hoechst 33342 (1:500, Life Technologies, H3570), for 1 min, washed again in PBS, 3 × 5 min, mounted in Fluoromount Aqueous Mounting Medium (Sigma, F4680), and left to dry overnight before imaging.

Images were acquired on a Zeiss LSM 710 laser scanning confocal microscope. Setting for laser power, gain and offset were kept constant for each experiment. All images for quantification were taken through the 20× objective (numerical aperture 0.40). Images were analyzed using the spots function on the Imaris 8 (Bitplane) software. Each marker was counted independently before overlaying images to observe co-distribution or to calculate as a percentage of total Hoechst-labeled nuclei. Two separate experimenters analyzed four sections/mouse from six control and six NCK1$^{-/-}$ mice. Experimenters were blind to the genotype during every step of this process.

Ethynyl deoxyuridine (EdU) proliferation and migration assays

Two groups of pregnant NCK1 heterozygous dams received intraperitoneal injections of EdU (10 µl/g) at E14.5. Group 1 was killed by cervical dislocation 30 min after injection, embryos were dissected, fixed (4% PFA, 45 min), washed (PBS, 3 × 20 min), cryoprotected (30% sucrose, 48 h). Coronal sections (20 µm) were cut and mounted onto charged slides (Fisher brand Superfrost Plus). Mice in group 2 were returned to their cages after injection until E18.5 when the brains of the E18.5 embryos were dissected and the same procedures as above were followed.

Slides of coronal sections were then treated according to manufacturer's instructions for the Click-iT EdU Alexa Fluor 647 Imaging kit (Life Technologies, C10340). Images were acquired on a Zeiss LSM 710 laser scanning confocal microscope and displayed using ZEN2009 software. The setting for laser power, gain and offset were kept constant for each experiment. All images for quantification were taken through the 20× objective (numerical aperture 0.40) in the hippocampal formation at E14.5 and in the hippocampus at E18.5. Images were analyzed using the spots function on the Imaris 8 (Bitplane) software. Each marker was counted independently before overlaying images to calculate the amount of EdU-positive cells as a percentage of total Hoechst-labeled nuclei. Two separate experimenters analyzed four sections/mouse from 6 control and 6 NCK1$^{-/-}$ mice at both E14.5 and E18.5 time points. Experimenters were blind to the genotype during every step of this process.

Golgi's method and dendritic spine analysis

Male mice received a lethal injection of sodium pentobarbital (2.4 mg/g, i.p.; Bimeda-MTC Animal Health Inc.), brains were dissected and whole brains were immersed in the Golgi impregnation solutions for two weeks in FD Rapid Golgi Stain kit (FD Neurotechnologies) and tissue preparation and staining procedure was done following the manufacturer's protocol.

Images were acquired on a Leica DM2000 microscope and displayed using QCapture Suite PLUS software. Images for Sholl analysis were taken with a 20× objective. Sholl analysis (Sholl, 1953) was conducted on ImageJ and consisted of a series of concentric circles 20 µm apart where the center circle was placed over the neuron's soma. Images for dendritic spine quantification were taken from the basal dendrites of the CA1 pyramidal neurons through the 100× objective. Images were analyzed and spines were counted using ImageJ software and the cell counter plugin. Two separate experimenters analyzed 20 dendrites/mouse from control and NCK1$^{-/-}$ mice. Experimenters were blind to the genotype during every step of this process.

qPCR

Total RNA was isolated from adult mouse hippocampus using TRIzol reagent (Invitrogen, Life Technologies), and reverse-transcribed with SuperScript III Reverse Transcriptase (Invitrogen) according to manufacturer's instructions. Quantitative PCR (qPCR) conditions were developed according to the manufacturer's protocol for SsoFast EvaGreen Supermix kit (Bio-Rad Laboratories). To demonstrate the expression level of each isoform, the threshold cycle (C_T) value of Cyclophilin A was used to normalize the expression level by using the $2^{-\Delta\Delta Ct}$ method.

The following primers were chosen for qPCR:

Nck1-1L: 5′-GCTGAAGAAGTGGTGGTGGT-3′
Nck2-1R: 5′-AGATGCTTTCCGAGCACTGT-3′
Nck2_23: 5′-AGGACAGGCTACGTGCCTT-3′
NCK2_24: 5′-GTACTCCGCATCAGTGCTTGG-3′
Cyclophilin A-5A: 5′-GAGCTGTTTGCAGACAAAGTT-3′
Cyclophilin A-3A: 5′-CCCTGGCACATGAATCCTGG-3′

Transmission electron microscopy (TEM)

Male mice received a lethal injection of sodium pentobarbital (2.4 mg/g, i.p.; Bimeda-MTC Animal Health Inc.) and the dorsal CA1 region of their hippocampi were dissected. Samples were fixed (2.5% glutaraldehyde in 0.1 M sodium cacodylate buffer, 2 h), rinsed (3× sodium cacodylate buffer, 10 min), fixed again (1% osmium tetroxide, 2 h), rinsed quickly (distilled water), incubated (0.25% uranyl acetate, 4°C overnight), dehydrated (graduated series of acetone, 50% acetone 10 min, 2 × 70% acetone 10 min, 2 × 95% acetone 10 min, 2 × 100% acetone 10 min, dried 100% acetone 10 min), infiltrated (epon Araldite resin, 3:1 acetone:resin 3 h, 1:3 acetone:resin overnight, 2 × 100% epon Araldite resin 3 h), and embeded (100% epon Araldite resin, 60°C 48 h); 100-nm sections were cut using a Reichert- Jung Ultracut E. Ultramicrotome with a diamond knife and placed on 300 mesh copper grids. Sections were stained in a solution of 2% aqueous uranyl acetate 10 min, 2× distilled water rinse 5 min, lead citrate 4 min, quick rinse distilled water, then air dried. Samples were viewed using a JEOL JEM 1230 transmission electron microscope at 80 kV. Images were captured using a Hamamatsu ORCA-HR digital camera. Images for synapse density counts were taken at 15,000× magnification. Six fields/animal were quantified using ImageJ software for four controls and five NCK1$^{-/-}$. For postsynaptic density area analysis, area was calculated using ImageJ for 10–15 synapses/animal. Experimenters were blind to the genotype during every step of this process.

Dissociated hippocampal culture preparation and *in vitro* immunocytochemistry

Dissociated hippocampal neurons from NCK1$^{+/-}$ (heterozygous, control) and NCK1$^{-/-}$ mice were prepared as previously described (Quinn et al., 2019). For immunocytochemistry, cultures were fixed with 4% paraformaldehyde, 4% sucrose at room temperature for 3 min followed by methanol at 4°C for 10 min, washed with PBS, transferred onto Parafilm wax, and blocked with 1% bovine serum albumin in PBS for 1 h. Primary antibodies were diluted in blocking solution and applied for 24 h at room temperature. Coverslips were then washed with PBS and blocked for 30 min. Fluorescently labeled secondary antibodies were diluted in blocking solution and applied for 1 h at room temperature, and coverslips were washed with PBS and mounted onto slides with Fluoromount (Sigma). Primary antibodies included Homer1 (rabbit polyclonal, Synaptic Systems, lot #160002, 1:3000) and MAP2 (guinea pig polyclonal, Synaptic Systems, lot #188004, 1:400). Secondary antibodies were DyLight 549 (donkey anti-rabbit, Thermo Fisher Scientific, 1:400), AMCA (donkey anti-guinea pig, Jackson Labs, 1:400).

cDNA constructs

The cDNA for mouse NCK1-myc was purchased from Origene (MR205875). To generate NCK1-mGFP, mGFP was amplified with forward and reverse primers encoding MluI and XhoI sites respectively. The mGFP MluI/XhoI fragment was then ligated into the NCK1-myc vector via unique MluI/XhoI sites to create NCK1-GFP. Synaptophysin was cloned from rat via RT-PCR. Mouse Homer1B was a gift from Carlo Sala. Open reading frames for Synaptophysin and Homer1b were fused to the 5′ and 3′ ends, respectively, of mCherry cDNA contained in an expression vector derived from pEGFP-C1 (Clontech) to create Synaptophysin-mCherry and mCherry-Homer1b. LV-GFP-β-actin was created by first replacing the CMV promoter in the lentivirus competent vector, pGIPZ-CMV-tGFP (Horizon Discovery) with a synapsin promoter using standard PCR-based cloning techniques. We then replaced tGFP with pEGFP–β-actin, provided by Roy Duncan (Dalhousie University, Halifax, Canada), to create pGIPZ-Syn-GFP-Actin. Synaptophysin-pHluorin (SypHl) has been previously described (Matz et al., 2010).

Lentivirus production

HEK293T cells were transfected with a mixture of envelope plasmid pmd2.G, packaging plasmid psPAX2, and LV-GFP-β-actin at a ratio of 1.2:3:5.8 (w/w/w) and linear poly(ethyleneimine; Polysciences Inc.). Plasmids pmd2.G and psPAX2 were gifts from Didier Trono (Addgene plasmids 12259 and 12260). HEK293T cells were incubated in DMEM containing the transfection mix for 5 h, then fresh DMEM with 5% fetal bovine serum (FBS) was added for 2 d. Virus-containing medium was collected, filtered through a 0.45-µm sterile filter, and concentrated 50-fold using 100-kDa molecular weight cutoff centricon filters (Pall). Concentrated virus stocks were stored at −80°C.

In vitro synapse density assay

Hippocampal neurons prepared as previously described (Quinn et al., 2019) from NCK1$^{+/-}$ (heterozygous, control) and NCK1$^{-/-}$ mice were fixed at days in vitro (DIV) 14–15 and immunostained for Homer1 to label excitatory postsynaptic specializations and MAP2 to label dendrites. Image stacks comprising five images over a z-distance of 1.75 µm were acquired with a Zeiss Observer 2.1 inverted microscope using a 63× objective, Photometrics Coolsnap HQ2 camera and SlideBook 6 imaging software. Maximum intensity projection images were created and Homer1 puncta were detected with a custom script using IVision software. For each neuron, two to four primary dendrites were selected using the MAP2 image, and Homer1 puncta within 10–100 µm from the soma were counted. Homer1 puncta >3 µm from primary dendrites were excluded from analysis. Images from three separate control and NCK1$^{-/-}$ cultures were analyzed. The experimenter was blinded to experimental conditions during image acquisition and analysis.

Fluorescent synaptic enrichment assay

To test whether exogenous NCK localizes to presynaptic or postsynaptic compartments, we compared the enrichment of NCK-GFP at synaptic sites to that of cytosolic GFP. To examine presynaptic enrichment, we co-expressed the presynaptic vesicle marker, synaptophysin-mCherry (Syph-mCh) along with GFP or NCK1-GFP in DIV 12 dissociated rat hippocampal neurons and imaged 2 d later. For each presynaptic site, we used the Syph-mCh image to select regions of interest (ROIs) on the synaptic bouton and nearby axonal shaft. ROIs were then overlain on the GFP/NCK1-GFP images, and the bouton-to-axon fluorescent ratio was measured for each synapse and averaged for each neuron. Presynaptic enrichment ratios for cytosolic GFP and NCK1-GFP-expressing neurons were statistically compared using a Student's *t* test.

To examine postsynaptic enrichment of NCK1-GFP we co-expressed the postsynaptic marker, mCherry-Homer (mCh-Hmr) along with GFP or NCK1-GFP in DIV 12 dissociated rat hippocampal neurons and imaged 2 d later. For each dendritic spine, we used the mCh-Hmr image to select ROIs on the dendritic spine and nearby dendritic shaft. ROIs were then overlain on the GFP/NCK1-GFP images, and the spine-to-shaft fluorescent ratio was measured for each synapse and averaged for each neuron. Postsynaptic enrichment ratios for cytosolic GFP and NCK1-GFP-expressing neurons were statistically compared using a Student's *t* test.

Assessment of presynaptic function with synaptophysin-pHluorin

To test whether presynaptic function was perturbed by loss of NCK1, we used a genetically encoded optical sensor for synaptic vesicle exocytosis called Synaptophysin-pHluorin (SypHl). Dissociated hippocampal cultures made from NCK Het and NCK1 KO mice were transfected with 70 µg of SypHl at DIV 12 and fluorescence microscopy was conducted on a Nikon TE2000 epifluorescence microscope equipped with a 60× (N.A. 1.40) objective, Smart shutter (Sutter Instruments) and Lumencor solid-state illumination at DIV 14–15. Images were acquired at 10 Hz with a Hamamatsu ORCA CCD camera and IPLab software. Experiments were performed at 36 ± 2°C in HBS solution [110 mM NaCl, 5.3 mM KCl, 2 mM $CaCl_2$, 1 mM $MgCl_2$, 20 mM 4-(2-hydroxyethyl)−1-piperazineethanesulfonic acid (HEPES), and 25 mM D-glucose adjusted to pH 7.30] supplemented with 10 μM 6,7-dinitroquinoxaline-2,3-dione (DNQX) and 50 μM (2R)-amino-5-phosphonovaleric acid (APV) to prevent recurrent excitation. Axons were selected based on basal SypHl fluorescence, and SypHl fluorescence changes (ΔF) were measured in response to field stimulation employing 1-ms square current pulses yielding electrical fields of ~10 V/cm through platinum electrodes placed 0.5 cm apart. Image acquisition and extracellular stimulation were synchronized using a Master-8 stimulator (AMPI). Stimulus trains of 80 stimuli at 80 Hz were given to measure the readily releasable pool (RRP) of synaptic vesicles. Images were acquired from five different NCK$^{+/-}$ hippocampal cultures and four different NCK1$^{-/-}$ hippocampal cultures. Images were background-subtracted and aligned using iVision software (BioVision). ROIs for measurement were selected on SypHl ΔF images according to a threshold-based algorithm. Synaptic regions of measurement had a size between 0.32 and 0.64 μm^2. For each experimental field, the average synaptic SypHl ΔF response was calculated. Differences in ΔF responses between NCK$^{+/-}$ and NCK1$^{-/-}$ groups were statistically tested using Student's *t* tests for independent samples.

Preparation of PSD fractions

Brain from male and female adult rats were collected and stored at –80°C until use. Isolation of PSD fractions from rat was performed as described previously (Wigerius et al., 2018). Briefly, the LP1 fraction containing synaptosomes was layered on top of a discontinuous sucrose gradient and centrifuged at 150 000 × *g* for 2 h. The membrane fraction was collected at the 1 and 1.2 M sucrose interface, and the suspension was centrifuged at 200 000 × *g* for 30 min to yield the synaptic plasma membrane fraction (SPM). The SPM fraction was treated with 0.5% Triton X-100 and centrifuged at 32,000 × *g* for 20 min to obtain the PSD fraction. The final PSD pellet was stored at –80°C until use and resuspended in 0.5% Triton X-100 before SDS-PAGE and immunoblot analysis.

SDS-PAGE and immunoblotting

Protein concentrations were measured using the bicinchoninic assay method (Thermo Fisher Scientific), and 10–20 µg of protein per lane

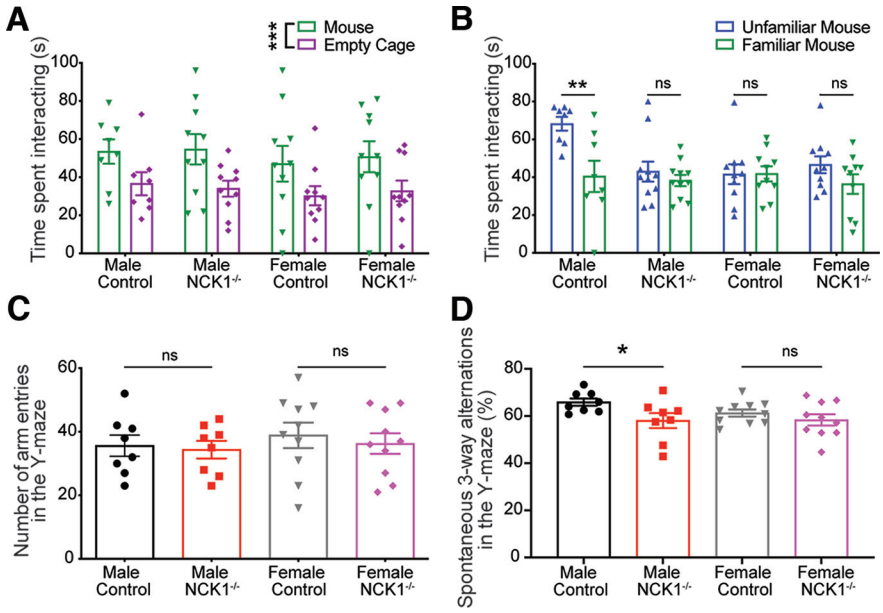

Figure 1. Sociability, short-term memory, and working memory assessment in mice deficient in NCK1 and their wild-type littermates. ***A***, Time spent interacting with an unfamiliar mouse and an empty cage during a three chambered social interaction task by male control ($n = 8$), male NCK1$^{-/-}$ ($n = 10$), female control ($n = 10$), and female NCK1$^{-/-}$ ($n = 10$) mice. Error bars represent mean ± SEM; ***$p < 0.001$ (three-way ANOVA). ***B***, Time spent interacting with a familiar mouse and an unfamiliar mouse during a three chambered social recognition task by male control ($n = 8$), male NCK1$^{-/-}$ ($n = 10$), female control ($n = 10$), and female NCK1$^{-/-}$ ($n = 10$) mice. Error bars represent mean ± SEM; **$p < 0.01$, ns (not significant) $p > 0.05$ (three-way ANOVA followed by Sidak's multiple comparisons test). ***C***, Number of arm entries in the Y-maze of male control ($n = 8$), male NCK1$^{-/-}$ ($n = 8$), female control ($n = 10$), and female NCK1$^{-/-}$ ($n = 10$) mice. Error bars represent mean ± SEM; ns (not significant) $p > 0.05$ (two-way ANOVA followed by Sidak's multiple comparisons test). ***D***, Percentage of spontaneous three-way arm alternations in the Y-maze of male control ($n = 8$), male NCK1$^{-/-}$ ($n = 8$), female control ($n = 10$), and female NCK1$^{-/-}$ ($n = 10$). Error bars represent mean ± SEM; *$p < 0.05$ (two-way ANOVA followed by Sidak's multiple comparisons test).

was loaded for SDS-PAGE. For immunoblots, the following primary antibodies were used: monoclonal PSD95 (1:500; Ab 2723; Abcam), Synaptophysin (1:5000; S-5678; Sigma-Aldrich). NCK1 was detected with a GST-fusion antibody raised against the 3 NCK1 SH3 domains (1:5000, gift from Tony Pawson). Secondary Horse-radish- peroxidase conjugated anti mouse (Sant Cruz Biotechnology) and rabbit (Bio-Rad) were used at 1:5000. Membranes were visualized using the digital ChemiDoc system (Bio-Rad).

Fluorescence recovery after photobleaching (FRAP) assay

Photobleaching imaging

FRAP experiments were performed as described previously (Wigerius et al., 2018). Briefly, imaging was conducted on a spinning-disk microscope (Zeiss) using a 63 × 1.4 NA oil immersion lens with a stage incubator (37°C and 5% CO_2). Dendritic spines on NCK1$^{+/-}$ and NCK1$^{-/-}$ hippocampal neurons infected with lentiviral particles expressing GFP-β-actin (LV-GFP-actin) for 3–4 d were photobleached and imaged without or with Jasplakinolide (J4580; Sigma-Aldrich). To monitor turnover, a ROI with a diameter of ~1 µm was photobleached at full laser power (100% power and 100% transmission) for 2.5 s. Fluorescence recovery was monitored by automatic scanning of the whole cell in 0.2-s intervals at low laser power. During image processing the mean fluorescence of an un-transfected area was measured as background and subtracted from the intensity of each frame to obtain recovery plots in ImageJ (NIH). The data were fit by nonlinear regression to an exponential one-phase association model in Prism (GraphPad software). The time for GFP-β-actin fluorescence to recover to 50% of its initial value (halftime recovery) was estimated directly from the recovery plots and the mobile fraction (M_f), expressed as a percentage, was approximated by a photobleach correction equation (Feder et al., 1996; Lippincott-Schwartz et al., 1998). Results were presented by bar graphs made with Prism.

Actin barbed end experiments and imaging

For the visualization of actin barbed ends a previously described protocol was used (Gu et al., 2010). Briefly, mouse hippocampal neurons infected with LV-GFP-actin were incubated with 0.45 µM rhodamine-conjugated G-actin (Rh-actin, Cytoskeleton Inc.) for 2 min in saponin permeabilization buffer (20 mM HEPES, 138 mM KCl, 4 mM $MgCl_2$, 3 mM EGTA, 0.2 mg/ml saponin, 1 mM ATP, and 1% BSA, pH 7.5). Neurons on coverslips were immediately fixed in cytoskeleton buffer, mounted on microscope slides and prepared for imaging. Images were acquired as z stack series taken at optimal step intervals with an LSM710 confocal scanning microscope using a 63× 1.4 NA oil immersion lens and collected with a digital Axiocam camera controlled by ZEN software (Zeiss). To analyze incorporation of spine rhodamine-actin, z stack images were collapsed by maximum-intensity projection using ImageJ (NIH). Dendritic spines were identified by generating masks of regions of interest (ROIs) applied along GFP-actin expressing dendritic segments that were overlaid on dendritic segments expressing Rh-actin. Both channels were equally thresholded and actin in dendritic spines was assessed by measuring the ratio of spine to shaft fluorescence intensity of Rhodamine normalized to GFP, as previously described (Wigerius et al., 2018).

Statistical analysis

All data are expressed as means ± SEM and all statistics were analyzed using Prism 8 or 9 (GraphPad Software). Independent Student's *t* tests were used for analysis of differences between two groups. When comparing more than two groups, ANOVA and Tukey's *post hoc* tests were used. Two-way ANOVA was used when multiple conditions were compared with multiple genotypes or sex. A three-way ANOVA was used when comparing testing condition, genotype, and sex. To monitor changes over time, repeated measures ANOVA were run followed by Sidak's multiple comparisons test. Statistical significance was set at $p < 0.05$.

Results

NCK1 deficiency impairs short-term and working memory

Given that NCK1 is expressed in the brain, is implicated in actin cytoskeletal rearrangement, and that the regulation of the actin cytoskeleton is associated with memory and learning, we asked whether mice lacking NCK1 have defects in learning and memory tasks. Our previous work showed that loss of NCK1 does not affect sensory or motor function (Diab et al., 2020). However, whether loss of NCK1 results in disruptions in social recognition, short-term memory, or spatial memory has not been addressed. We first tested whether loss of NCK1 affected social interactions and social recognition using the Crawley's three-chambered social interaction paradigm (Moy et al., 2004). Here, all mice, regardless of sex or genotype, spent significantly more time interacting with a caged mouse versus an empty cage (***$p = 0.0004$, two-way ANOVA; Fig. 1*A*). Therefore, NCK1 mutant mice behave as control mice and do not show deficits in this sociability paradigm.

One hour following the social interaction task, mice were tested for social recognition, a form of short-term memory (Moy et al., 2004; Richter et al., 2005). In the social recognition task, as

expected, male control mice spent more time interacting with the unfamiliar mouse than with the familiar mouse (68.3 ± 7.7 vs 40.5 ± 7.7 s, $n = 8$, $^{**}p = 0.0024$, three-way ANOVA followed by Sidak's multiple comparisons test; Fig. 1*B*). However, the male NCK1$^{-/-}$ mice failed to differentiate between the unfamiliar and familiar mice (male NCK1$^{-/-}$ 43.0 ± 6.6 vs 38.3 ± 6.6 s, $n = 11$, $p = 0.9240$, three-way ANOVA followed by Sidak's *post hoc* comparison test; Fig. 1*B*). These data are consistent with defects in short-term memory in the male NCK1 mutant mice. Our protocol was unsuccessful in female mice since both control and mutant female mice did not differentiate between the unfamiliar and familiar mice (female control 41.6 ± 6.9 vs 41.8 ± 6.9 s, $n = 10$, $p > 0.9999$, female NCK1$^{-/-}$ 46.6 ± 6.9 vs 36.4 ± 6.9 s, $n = 10$, $p = 0.4627$, three-way ANOVA followed by Sidak's *post hoc* comparison test; Fig. 1*B*).

To further assess for memory deficits, male and female NCK1$^{-/-}$ and their littermate controls were challenged in the Y-maze, a test for spatial working memory (Kraeuter et al., 2019). All mice had similar levels of exploratory activity (male control, 35.6 ± 5.2 arm entries, $n = 8$ vs male NCK1$^{-/-}$, 34.4 ± 5.2 arm entries, $n = 8$, $p = 0.9642$, and female control 38.9 ± 4.6 arm entries, $n = 10$ vs 36.3 ± 4.6 arm entries, $n = 10$, $p = 0.8223$, ordinary one-way ANOVA followed by Sidak's multiple comparisons test; Fig. 1*C*). However, male NCK1$^{-/-}$ mice showed a decrease in their spontaneous three-way alternations compared with control mice (male control 65.9 ± 3.3% three-way alternations, $n = 8$, vs male NCK1$^{-/-}$ 58.1 ± 3.3% three-way alternations, $n = 8$; $^{*}p = 0.0492$, ordinary one-way ANOVA followed by Sidak's multiple comparisons test; Fig. 1*D*). Unlike the male mice, female control and NCK1$^{-/-}$ mice preformed similarly in the Y-maze (female control 61.3 ± 3.0% three-way alternations, $n = 10$ vs female NCK1$^{-/-}$ 58.3 ± 3.0% three-way alternations, $n = 10$, $p = 0.5452$, ordinary one-way ANOVA followed by Sidak's multiple comparisons test). Thus, although all mice showed similar total arm entries, male mice deficient in NCK1 spent less time alternating between all three arms relative to their controls suggesting a reduced working memory capacity in the male mutant mice.

NCK1 deficiency impairs spatial learning and memory formation

We next tested the mice's spatial learning and memory abilities in a more complex paradigm using the Morris water maze. As the Morris water maze is dependent on swimming ability and vision, we tested for escape latency during visible platform trials in control and mutant mice and found similar average escape times (male control, 9.3 ± 3.5 s, $n = 12$; male NCK1$^{-/-}$, 10.2 ± 3.5 s, $n = 12$; female control, 17.3 ± 3.6 s, $n = 10$; female NCK1$^{-/-}$, 11.4 ± 3.6 s, $n = 10$; $p = 0.1174$, ordinary one-way ANOVA), suggesting that control and NCK1$^{-/-}$ mice have similar visual and swimming ability.

Our testing paradigm consisted of a 4-d acquisition phase, where the platform was first hidden in the northwest quadrant, followed by a 4-d reversal learning phase, where the platform was moved and hidden it in the southeast quadrant, and finally a platform-free probe trial on the ninth day. During the acquisition phase, male and female control mice as well a female NCK1$^{-/-}$ mice showed a significant decrease in the average escape latency by day 4 of training [male control mice, day 1, 36.3 ± 4.6 s vs day 4, 21.1 ± 3.2 s, $n = 24$, $^{*}p = 0.0232$, two-way ANOVA followed by Sidak's multiple comparisons test (Fig. 2*A*); female control mice, day 1, 39.4 ± 4.2 s vs day 4, 18.1 ± 4.2 s, $n = 20$, $^{****}p < 0.0001$, two-way ANOVA followed by Sidak's multiple comparisons test (Fig. 2*B*); female NCK1$^{-/-}$ mice, day 1, 38.8 ± 4.3 s vs day 4, 20.5 ± 4.3 s, $n = 20$, $^{***}p = 0.0002$, two-way ANOVA followed by Sidak's multiple comparisons test (Fig. 2*B*)]. However, male NCK1$^{-/-}$ mice showed no significant change in their average escape latency by day 4 of the acquisition phase (male NCK1$^{-/-}$ mice, day 1, 37.7 ± 3.7 s vs day 4, 24.7 ± 4.6 s, $n = 20$, $p = 0.1105$, two-way ANOVA followed by Sidak's multiple comparisons test; Fig. 2*A*), suggesting that control and female NCK1$^{-/-}$ mice, but not male NCK1$^{-/-}$ mice, are able to learn to locate the escape platform.

During the reversal learning phase, both male and female NCK1$^{-/-}$ mice fail to learn the task as there was no significant change in average escape latency by the final training day. This was not seen in their control littermates [male control mice, day 5, 35.4 ± 3.8 s vs day 8, 19.3 ± 4.3 s, $n = 24$, $^{*}p = 0.0435$, two-way ANOVA followed by Sidak's multiple comparisons test (Fig. 2*C*); male NCK1$^{-/-}$ mice, day 5, 31.9 ± 4.1 s vs day 8, 25.8 ± 4.1 s, $n = 20$, $p = 0.7953$, two-way ANOVA followed by Sidak's multiple comparisons test (Fig. 2*C*); female control mice, day 5, 45.0 ± 2.5 s vs day 8, 28.5 ± 2.5 s, $n = 20$, $^{*}p = 0.0288$, two-way ANOVA followed by Sidak's multiple comparisons test (Fig. 2*D*); female NCK1$^{-/-}$ mice, day 5, 39.2 ± 6.3 s vs day 8, 26.1 ± 6.3 s, $n = 20$, $p = 0.8569$, two-way ANOVA followed by Sidak's multiple comparisons test (Fig. 2*D*)]. Together, these data suggest that male NCK1$^{-/-}$ mice have deficits in both the memory acquisition and reversal learning in the Morris water maze, while female NCK1$^{-/-}$ mice have deficits in the reversal learning phase.

To further examine whether the differences in escape latencies were accurately reflecting the mice's ability to learn and remember the location of the hidden platform, we next assessed the percentage of time the mice spent in the quadrant containing the platform and compared it to the percentage of time spent in the opposing quadrant. By the third and fourth day of the acquisition phase, the male control mice spent a significantly greater percentage of time in the platform-containing northwest quadrant (NW) when compared with the southeast quadrant (SE; male control mice, day 3, NW 31.8 ± 2.4% vs SE 16.4 ± 2.0%, $n = 24$, $^{**}p = 0.0018$, two-way ANOVA followed by Sidak's multiple comparisons test, and day 4, NW 35.7 ± 4.0% vs SE 15.4 ± 2.1%, $n = 24$, $^{****}p < 0.0001$, two-way ANOVA followed by Sidak's multiple comparisons test; Fig. 2*E*). However, male NCK1$^{-/-}$ mice spent a similar percentage of time in the NW and SE throughout the acquisition phase including on days 3 and 4 (day 3, NW 29.2 ± 4.3% vs 18.2 ± 2.5%, $n = 20$, $p = 0.3196$, two-way ANOVA followed by Sidak's multiple comparisons test; and day 4, NW 29.0 ± 4.4% vs 26.6 ± 4.7%, $n = 20$, $p > 0.9999$, two-way ANOVA followed by Sidak's multiple comparisons test; Fig. 2*F*). On day 5 when the platform changes location from NW to SE, the male control mice spent increased time in the NW when compared with the amount of time spent in the SE, suggesting that they were searching for the platform in the NW (male control, NW 35.9 ± 2.5% vs 16.3 ± 1.7%, $n = 24$, $^{****}p < 0.0001$, two-way ANOVA followed by Sidak's multiple comparisons test; Fig. 2*E*), however, the male NCK1$^{-/-}$ mice do not (NW, 28.2 ± 3.2% vs 15.8 ± 2.1%, $n = 20$, $p = 0.0637$, two-way ANOVA followed by Sidak's multiple comparisons test; Fig. 2*F*). Additionally, on the final day of the reversal learning phase (day 8) and during the platform-free probe trial (day 9), the male control mice spent increased time in the platform-containing southeast quadrant (SE) when compared with the northwest quadrant (NW; male control mice, day 8, SE 33.7 ± 3.1% vs NW 18.8 ± 2.4%, $n = 24$, $^{**}p = 0.0029$, two-way ANOVA followed by Sidak's multiple comparisons test, and probe trial SE 34.8 ± 3.3% vs

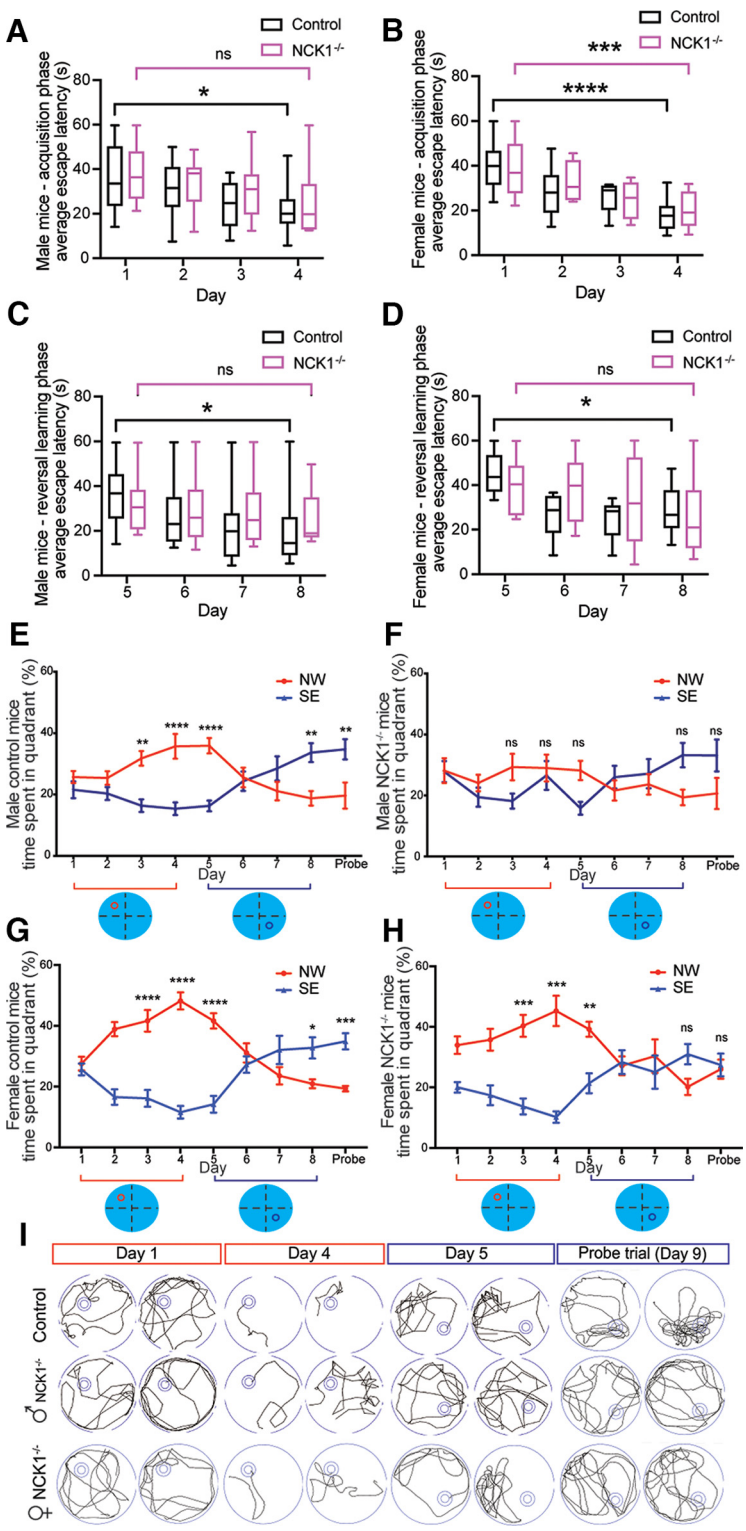

Figure 2. Assessment of spatial learning and memory in the Morris water maze of control and NCK1-deficient mice. ***A***, Average escape latency of male control (black, $n = 12$) and male NCK1$^{-/-}$ (magenta, $n = 10$) mice in the Morris water maze (MWM) over 4 d of acquisition testing. Magenta brackets indicate NCK1$^{-/-}$ group comparisons. Black brackets indicate control group comparisons. ns (not significant) $p > 0.05$, $^{*}p < 0.05$ (two-way ANOVA followed by Sidak's multiple comparisons test). ***B***, Average escape latency of female control (black, $n = 10$) and female NCK1$^{-/-}$ (magenta, $n = 10$) mice in the MWM over 4 d of acquisition testing. Magenta brackets indicate NCK1$^{-/-}$ group comparisons. Black brackets indicate control group comparisons. $^{***}p < 0.001$, $^{****}p < 0.0001$ (two-way ANOVA followed by Sidak's multiple comparisons test). ***C***, Average escape latency of male control (black, $n = 12$) and male NCK1$^{-/-}$ (magenta, $n = 10$) mice in the Morris water maze (MWM) over 4 d of reversal learning testing. Magenta brackets indicate NCK1$^{-/-}$ group comparisons. Black brackets indicate control group comparisons. ns (not significant) $p > 0.05$, $^{*}p < 0.05$ (two-way ANOVA followed by Sidak's multiple comparisons test). ***D***, Average escape latency of female control (black, $n = 10$) and female NCK1$^{-/-}$ (magenta, $n = 10$) mice in the MWM over 4 d of reversal learning testing. Magenta brackets indicate NCK1$^{-/-}$ group comparisons. Black brackets indicate control group comparisons. ns (not significant) $p > 0.05$, $^{*}p < 0.05$ (two-way ANOVA followed by Sidak's multiple comparisons test). ***E***, Percentage of time spent by male control mice ($n = 12$) in the northwest quadrant (NW, red) and southeast quadrant (SE, blue) over 9 d of testing in the MWM. Diagram indicates that the platform was hidden in the NW on days 1–4, and in the SE on days 5–8. Error bars represent mean ± SEM; $^{**}p < 0.01$, $^{****}p < 0.0001$ (two-way ANOVA followed by Sidak's multiple comparisons test). ***F***, Percentage of time spent by the male NCK1$^{-/-}$ mice ($n = 10$) in the NW (red) and SE (blue) over 9 d of testing. Diagram indicates that the platform was hidden in the NW on days 1–4, and in the SE on days 5–8. Error bars represent mean ± SEM; ns (not significant) $p > 0.05$ (two-way ANOVA followed by Sidak's multiple comparisons test). ***G***, Percentage of time spent by female control mice ($n = 10$) in the northwest quadrant (NW, red) and southeast quadrant (SE, blue) over 9 d of testing in the MWM. Diagram indicates that the platform was hidden in the NW on days 1–4, and in the SE on days 5–8. Error bars represent mean ± SEM; $^{*}p < 0.05$, $^{***}p < 0.001$, $^{****}p < 0.0001$ (two-way ANOVA followed by Sidak's multiple comparisons test). ***H***, Percentage of time spent by the female NCK1$^{-/-}$ mice ($n = 10$) in the NW (red) and SE (blue) over 9 d of testing. Diagram indicates that the platform was hidden in the NW on days 1–4, and in the SE on days 5–8. Error bars represent mean ± SEM; $^{**}p < 0.01$, $^{***}p < 0.001$, ns (not significant) $p > 0.05$ (two-way ANOVA followed by Sidak's multiple comparisons test). ***I***, Representative traces of swim-paths from male control (upper panel), and NCK1$^{-/-}$ (middle panel), and female NCK1$^{-/-}$ mice (lower panel) on day 1, day 4, day 5, and the probe trial (day 9) in the MWM.

NW 19.7 ± 4.3%, $n = 24$, $^{**}p = 0.0024$, two-way ANOVA followed by Sidak's multiple comparisons test; Fig. 2*E*); however, the male NCK1$^{-/-}$ mice do not (day 8, SE 33.2 ± 4.0% vs 19.4 ± 2.5%, $n = 20$, $p = 0.0892$, two-way ANOVA followed by Sidak's multiple comparisons test, and probe trial SE 33.1 ± 5.2% vs NW 20.7 ± 5.1%, $n = 20$, $p = 0.6316$, two-way ANOVA followed by Sidak's multiple comparisons test; Fig. 2*F*). This is consistent with male mice lacking NCK1 having impairments in learning spatial information in the Morris water maze.

Interestingly, female control and female NCK1$^{-/-}$ mice were able to learn during the initial acquisition phase as reflected in the percentage of time spent in the platform containing quadrant on the third, fourth, and fifth testing days (female control mice, day 3, NW 41.6 ± 3.5% vs SE 16.2 ± 2.8%, $n = 20$, $^{****}p < 0.0001$, two-way ANOVA followed by Sidak's multiple comparisons test, day 4, NW 48.2 ± 2.8% vs SE 11.6 ± 2.1%, $n = 20$, $^{****}p < 0.0001$, two-way ANOVA followed by Sidak's multiple comparisons test, day 5, NW 41.6 ± 2.5% vs SE 14.2 ± 2.8%, $n = 20$, $^{****}p < 0.0001$, two-way ANOVA followed by Sidak's multiple comparisons test, Fig. 2G; female NCK1$^{-/-}$ mice, day 3, NW 40.4 ± 3.6% vs SE 13.7 ± 2.6%, $n = 20$, $^{***}p = 0.0002$, two-way ANOVA followed by Sidak's multiple comparisons test, and day 4, NW 45.3 ± 5.0% vs SE 10.2 ± 1.9%, $n = 20$,

$^{***}p = 0.0003$, two-way ANOVA followed by Sidak's multiple comparisons test, day 5, NW 39.2 ± 2.5% vs 21.4 ± 3.3%, $n = 20$, $^{**}p = 0.0041$, two-way ANOVA followed by Sidak's multiple comparisons test; Fig. 2*H*). However, unlike the female control mice, the female NCK1$^{-/-}$ mice did not spend an increased percentage of time in the new platform containing quadrant during the reversal learning trials (days 5–8) or the probe trial [day 9; female control mice, day 8, SE 32.7 ± 3.5% vs NW 20.9 ± 1.5%, $n = 20$, $^{*}p = 0.0250$, two-way ANOVA followed by Sidak's multiple comparisons test, and probe trial SE 34.9 ± 2.7% vs NW 19.3 ± 0.9%, $n = 20$, $^{***}p = 0.0009$, two-way ANOVA followed by Sidak's multiple comparisons test (Fig. 2*G*); female NCK1$^{-/-}$ mice, day 8, SE 31.0 ± 3.3% vs NW 20.2 ± 2.7%, $n = 20$, $p = 0.1826$, two-way ANOVA followed by Sidak's multiple comparisons test, and probe trial SE 27.4 ± 3.7% vs NW 26.0 ± 3.2%, $n = 20$, $p > 0.9999$, two-way ANOVA followed by Sidak's multiple comparisons test (Fig. 2*H*)]. This supports the escape latency findings in Figure 2*D*, where we found that female mice lacking NCK1 had impairments in reversal learning in the Morris water maze.

Finally, when comparing the swim paths of control and NCK1$^{-/-}$ mice before and after the acquisition phase, on day 4 male control and female mice showed more directed swimming patterns toward the escape platform found in the NW quadrant, while male NCK1$^{-/-}$ mice showed a circling swimming pattern throughout the pool (Fig. 2*I*, second panel). The contrast in escape strategy was especially apparent when comparing swim paths on day 5 when the platform was moved from the NW to the SE. The swim paths of all control mice and female NCK1$^{-/-}$ mice were concentrated in the NW, while the male NCK1$^{-/-}$ mice's swim paths were not (Fig. 2*I*, third panel). However, during the probe trial (day 9), the swim paths of male and female control mice were concentrated in the SE, while the male and female NCK1$^{-/-}$ mice circled the pool more broadly (Fig. 2*I*, fourth panel). Together, these data suggest that both male and female NCK1-deficient mice have impairments in spatial learning and memory in the Morris water maze. However, male NCK1$^{-/-}$ mice have a more severe phenotype and fail at memory acquisition, while female NCK1$^{-/-}$ can learn the initial task but have impairments in reversal learning. Given the more severe learning and memory defects in the male NCK1$^{-/-}$ mice, subsequent analysis was restricted to male mice.

NCK1 is expressed in postmitotic neurons in the adult hippocampus

Our behavioral studies suggest that loss of NCK1 results in deficits in hippocampal dependent learning and memory. We therefore asked whether hippocampal defects in the NCK1$^{-/-}$ mice may contribute to these deficits. First, we asked whether NCK1 was present in the hippocampus, and in which cell types. Here, we took advantage of the IRES-β-galactosidase (β-gal) cassette that was inserted into the first coding exon of NCK1 and used β-gal expression as a proxy for endogenous NCK1 expression (herein NCK1^{+ve}). β-gal expression revealed that NCK1 is expressed throughout the hippocampus (Fig. 3*A*). To determine which cell types express NCK1, we co-labeled sections with β-gal, Hoechst (a nuclei marker), NeuN (a neuronal marker), Iba1 (a microglial marker), GFAP (an astrocyte marker), NG2 (an oligodendrocyte marker), and Sox2 (a progenitor cell marker). Throughout the hippocampus, we found that 98.8 ± 1.2% of the NeuN-positive cells were β-gal (NCK1)$^{+ve}$ (Fig. 3*B*) and 15.0 ± 1.6% of GFAP-positive cells were β-gal (NCK1)$^{+ve}$ (Fig. 3*C*). However, none of the Iba1-positive cells were β-gal (NCK1)$^{+ve}$ (Fig. 3*B*, arrows), nor was there any co-distribution with the oligodendrocyte marker NG2 (Fig. 3*D*) or with the progenitor cell marker Sox2 (Fig. 3*E*). Together, these data suggest that NCK1 is predominantly expressed in postmitotic neurons and in a subset of astrocytes but restricted from microglia and oligodendrocytes in the mature hippocampus. This is similar to our recent findings in the amygdala where almost all NeuN-positive cells express NCK1, but other cell types including microglia are lacking expression (Diab et al., 2020).

Loss of NCK1 does not impair hippocampal embryonic neuronal proliferation or migration

Although NCK1 was not detected in the Sox2 expressing progenitor cells in the adult dentate gyrus, others have implicated NCK proteins in cellular differentiation (Lu et al., 2015; Jacquet et al., 2018). Thus, we wanted to determine whether NCK1 was important for embryonic neuronal proliferation. Here, pregnant dames were injected with EdU, a thymidine analog that gets incorporated into the DNA of dividing cells, at E14.5, the height of hippocampal neurogenesis (Urbán and Guillemot, 2014). Embryos were then harvested 30 min after EdU injection as a measure of proliferation. In both control and NCK1$^{-/-}$ embryos there were similar levels of proliferation in the hippocampal neuroepithelium (22.3 ± 1.0% vs 24.3 ± 0.9%, $p = 0.1693$, $n = 12$, Student's t test; Fig. 4*A–E*). These results suggest that NCK1 is not necessary for neuronal proliferation in the hippocampal neuroepithelium.

Next, given that NCK1 has been implicated in cellular migration in other cellular contexts (Bladt et al., 2003; Chaki et al., 2013; Dubrac et al., 2018), we asked whether loss of NCK1 affects hippocampal neuronal migration. We monitored this by assessing EdU incorporation at E14.5 then waiting 4 d and scoring whether there were differences in the number and patterning of cells that migrated to form the embryonic hippocampus. We found similar fractions of EdU-labeled cells in the hippocampus of NCK1$^{-/-}$ and control embryos (Control 76.4 ± 4.2%, $n = 8$, vs NCK1$^{-/-}$ 74.4 ± 4.9%, $n = 6$, $p = 0.4420$, Student's t test; Fig. 4*F–J*). In addition, EdU-labeled cells in the NCK1$^{-/-}$ embryos displayed characteristic hippocampal patterning, similar to control, with a visible hippocampal fissure and a dense CA layer (Fig. 4*G*, *I*). These findings support our recent findings which demonstrated that NCK1 is not necessary for migration or proliferation in cortical tissues (Diab et al., 2020).

Loss of NCK1 results in decreased hippocampal dendritic spine density, decreased synapse-density, and increased PSD thickness *in vivo*

Given the impaired spatial learning and memory in the NCK1$^{-/-}$ mice but no gross abnormalities in embryonic development of the hippocampus, we next asked whether loss of NCK1 could affect neuronal morphology or synapse numbers in the adult hippocampus. Using Sholl analysis, we quantified the morphology of pyramidal neurons in the CA1 region of NCK1 mutant mice. Loss of NCK1 did not affect dendrite complexity of either the apical or basal dendritic arbors (Fig. 5*A*,*B*), suggesting that NCK1 is not critical for dendritic development of CA1 neurons.

Next, we assessed whether there were changes in synaptic density in the mutant mice using multiple methods. First, quantification of dendritic spine density using Golgi-stained preparations from control or NCK1$^{-/-}$ mice revealed an 18% decrease in dendritic spine density per 10 µm in pyramidal CA1 neurons of mutant mice relative to control (Control 19.3 ± 1.0 spines,

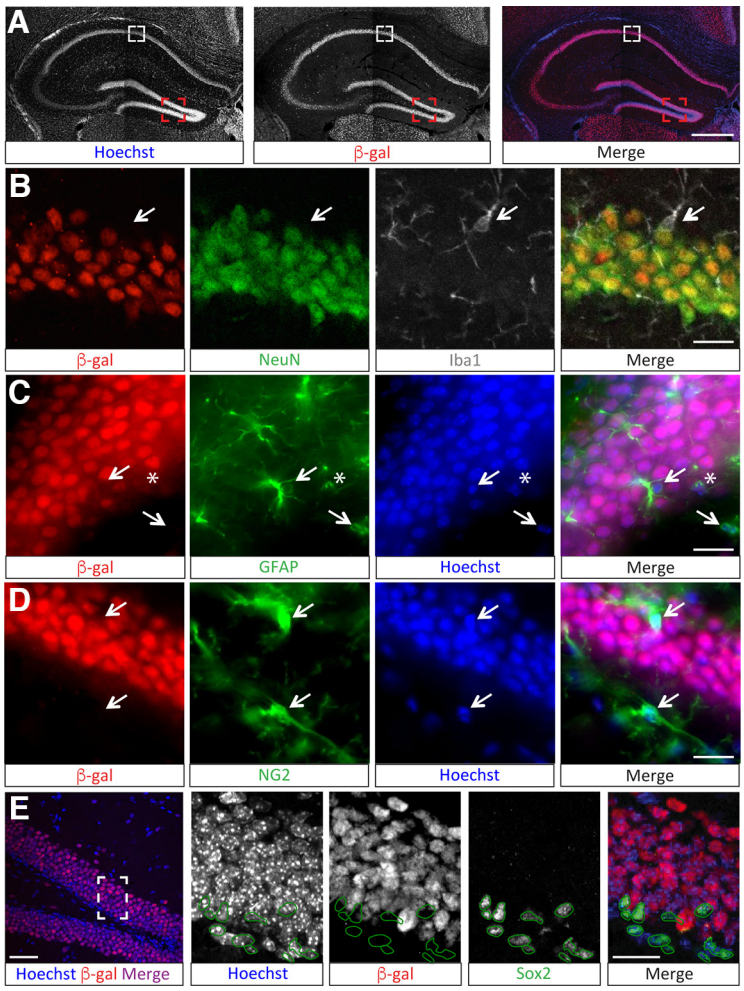

Figure 3. NCK1 expression in the hippocampus. ***A***, Confocal image of DNA marker Hoechst (blue)-labeled and β-gal (red)-labeled coronal section of the hippocampus of an NCK1 heterozygous ($NCK1^{+/-}$) mouse. White box outlines the representative area of the CA1 shown in the panels below. Red box outlines the representative area of the dentate gyrus shown in the C panels. Scale bar = 500 µm. ***B***, Magnification of the hippocampal CA1 region shown in ***A***. Immunostaining of the NCK1 proxy marker β-gal (red), together with neuron marker NeuN (green), and microglia marker Iba1 (gray). Merge panel shows overlap of β-gal and NeuN stain with arrows indicating Iba1-positive and β-gal-negative cell. Scale bar = 20 µm. ***C***, Hippocampal CA1 region immunolabelled for the NCK1 proxy marker β-gal (red), together with the astrocyte marker GFAP (green), and the nuclei marker (Hoechst). Merge panel shows overlap of the three channels. Arrows indicate GFAP-positive and β-gal-negative cells and the star indication a GFAP-positive, β-gal-positive cell. Scale bar = 20 µm. ***D***, Hippocampal CA1 region immunolabelled for the NCK1 proxy marker β-gal (red), together with the oligodendrocyte marker NG2 (green), and the nuclei marker (Hoechst). Merge panel shows overlap of the three channels. Arrows indicating NG2-positive and β-gal-negative cells. Scale bar = 20 µm. ***E***, Dentate gyrus of hippocampus. Middle panels show magnified region in ***E*** showing Hoechst, β-gal, and the progenitor cell marker, Sox2. Green circles outline Sox2-positive cells lacking β-gal immunoreactivity. Far right panel show merge of all channels. Scale bars = 50 µm (first panel) and 20 µm (last 4 panels).

$n = 5$, vs $NCK1^{-/-}$ 15.4 ± 0.9 spines, $n = 7$, $^{*}p = 0.0155$, one-way ANOVA followed by Tukey's multiple comparisons test; Fig. 5*C*, *D*). To test whether there was a gene dosage effect, we also quantified CA1 spine density in $NCK1^{+/-}$ mice and found that although there was a trend toward reduced spine density compared with wild-type littermates, there was no statistical significance (Control 19.3 ± 1.0 spines, $n = 5$, vs $NCK1^{+/-}$ 17.6 ± 0.7 spines, $n = 8$, $p = 0.3557$, one-way ANOVA followed by Tukey's multiple comparisons test; Fig. 5*D*). Nor was there any statistical difference between the $NCK1^{+/-}$ and $NCK1^{-/-}$ mice ($NCK1^{+/-}$ 17.6 ± 0.7 spines, $n = 8$, vs $NCK1^{-/-}$ 15.4 ± 0.9 spines, $n = 7$, $p = 0.1429$, one-way ANOVA followed by Tukey's multiple comparisons test; Fig. 5*D*).

As NCK2 has been proposed to play a functionally redundant role for the loss of NCK1 which may affect the severity of the phenotype (Bladt et al., 2003; Fawcett et al., 2007; Clouthier et al., 2015), we tested whether NCK2 was present in the hippocampus of $NCK1^{-/-}$ mice. We confirmed that NCK2 mRNA was expressed in the pyramidal cell layers in wild-type mice (Fig. 5*E*). Next, using qPCR, we found that despite NCK2 transcript being present, the levels were not affected by the loss of NCK1 compared with littermate controls (Fig. 5*F*). Whether the reduction in dendritic spine density is modulated in part by the presence of NCK2 protein in the hippocampus of the $NCK1^{-/-}$ remains to be tested.

In addition to the Golgi analysis, we quantified the density of asymmetric, excitatory synapses using transmission electron microscopy (TEM) on sections taken from the CA1 region of the dorsal hippocampus. Similar to our Golgi stain results, the TEM analysis showed a reduction in the number of postsynaptic densities per 10 μm^2 in the hippocampus of $NCK1^{-/-}$ mice when compared with control (Control 4.60 ± 0.22 synapses, $n = 18$, vs $NCK1^{-/-}$ 2.68 ± 0.24 synapses, $n = 29$, $^{****}p < 0.0001$, Student's t test; Fig. 6*A–C*). Together, these results suggest that NCK1 is necessary for normal synapse numbers.

We next assessed whether there were any changes in various PSD parameters (size, thickness, and length) in the mutant mice. Surprisingly, we found that $NCK1^{-/-}$ mice exhibited on-average larger PSD size when compared with control (Control, 6413 ± 461 nm^2, $n = 4$ vs $NCK1^{-/-}$ 9544 ± 815 nm^2, $n = 5$, $^{***}p = 0.0010$, Student's t test; Fig. 6*D–G*). The mutant mice had a significant increase in PSD thickness (Control 32.1 ± 1.9 nm, $n = 4$, vs $NCK1^{-/-}$ 39.7 ± 1.4 nm, $n = 5$, $^{*}p = 0.0135$, Student's t test; Fig. 6*H*) but not in PSD length ($NCK1^{-/-}$ 242.4 ± 17.2 nm, $n = 5$, vs Control 203.3 ± 24.6 nm, $n = 4$, $p = 0.2218$, Student's t test; Fig. 6*I*), suggesting that loss of NCK1 results in an expanded pallium. Taken together, loss of NCK1 results in decreased dendritic spine density and synapse numbers in the hippocampus, while synapses that are formed have normal dendritic spine morphology but larger PSD thickness.

NCK1 is localized to dendritic spines and loss of NCK1 results in decreased dendritic spine density and enhanced homer staining in cultured hippocampal neurons

Because of the decreased synapse density in the hippocampus of $NCK1^{-/-}$ mice, we sought to understand whether this loss was caused by a defect in actin filaments, which form the major structural framework of synapses. We first determined the localization of NCK1 in the synapse by isolating synaptosomes through differential centrifugation of whole brain lysate. NCK1 was detected in the supernatant (S1) and the crude synaptosomal membrane (LP1) fractions (Fig. 7*A*). Like the PSD marker PSD-95,

we also found NCK1 in the synaptic plasma membrane (SPM) fraction as well as in the Triton X-100 resistant PSD fraction (Fig. 7*B*), indicating that NCK1 is associated with the postsynaptic density.

To assess NCK1's function at the level of individual neurons, we cultured hippocampal neurons from control and NCK1-deficient embryos and quantified the dendritic complexity using Sholl analysis and found no differences in dendrite number or complexity between control and NCK1$^{-/-}$ neurons (Fig. 7*C*). Next, to better understand the subcellular localization of NCK1, we overexpressed GFP-NCK1 in dissociated hippocampal neurons. We found that GFP-NCK1 localized to dendrites and was enriched in dendritic spines along with the PSD marker Homer (Fig. 7*D*). Indeed, NCK1-GFP had a 69.9% increase in fluorescence intensity in dendritic spines when compared with GFP alone (****$p < 0.0001$, Student's *t* test; Fig. 7*E*). Presynaptically, NCK1-GFP was also found in axons and at synaptophysin-labeled synaptic boutons but at similar levels as GFP alone ($p = 0.9650$, Student's *t* test; Fig. 7*F*,*G*).

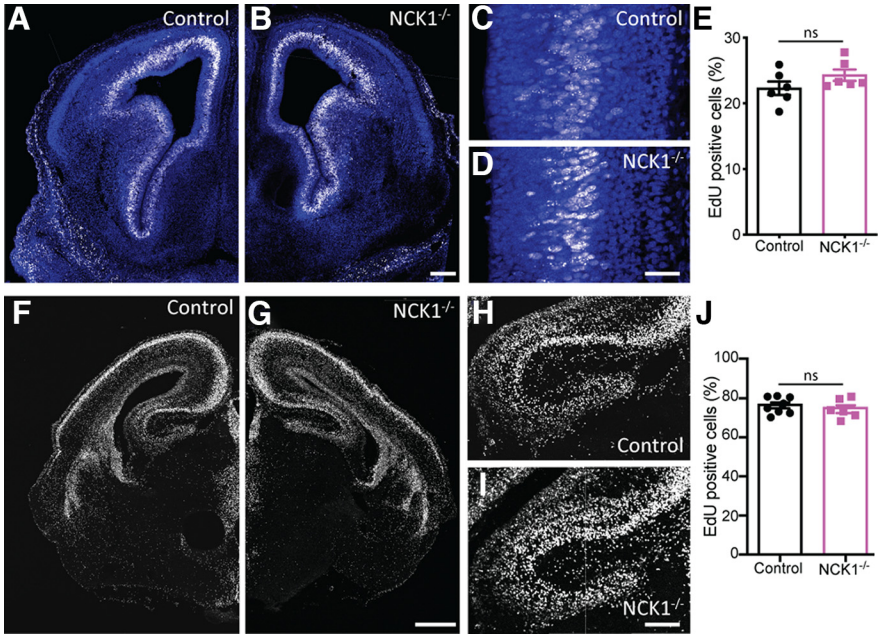

Figure 4. Analysis of cell proliferation and migration in the hippocampus of control and NCK1$^{-/-}$ embryos. ***A–D***, Confocal images of coronal sections of E14.5 brains and hippocampal epithelium that were EdU-labeled (white) at E14.5. Hoechst-labeled DNA in blue. ***E***, Quantification of the percentage of EdU-positive cells in the hippocampal epithelium of control ($n = 6$) and NCK1$^{-/-}$ ($n = 6$) embryos at E14.5. Error bars represent mean ± SEM; ns (not significant) $p > 0.05$ (Student's *t* test). Scale bars = 200 and 25 µm (second and third panels, respectively). ***F–I***, Confocal images of E18.5 brains and hippocampi that were EdU-labeled (white) at E14.5. ***J***, Quantification of the percentage of EdU-positive cells in the hippocampal formations of control ($n = 8$) and NCK1$^{-/-}$ ($n = 6$) embryos at E18.5. Error bars represent mean ± SEM; ns (not significant) $p > 0.05$ (Student's *t* test). Scale bars = 500 and 150 µm (second and third panels, respectively).

Further, to examine the effect of NCK1 deficiency on dendritic spine number and size, we analyzed Homer1 expression. Homer1 is a PSD scaffold protein with protein levels directly proportional to PSD size (Hayashi et al., 2009). We found that NCK1-deficient neurons had a 23.5% reduction in the density of Homer1-positive puncta per 10 µm (Control 7.20 ± 0.41 puncta, $n = 48$, vs NCK1$^{-/-}$ 5.51 ± 0.26 puncta, $n = 47$, ***$p = 0.0008$, Student's *t* test; Fig. 7*H*,*J*). However, NCK1$^{-/-}$ neurons had, on-average, a 13.2% increase in the fluorescent intensity of Homer1 puncta compared with control mice (Control 24.0 ± 5.0 × 10^3 A.U., $n = 36$, vs NCK1$^{-/-}$ 27.2 ± 6.0 × 10^3 A.U., $n = 36$, *$p = 0.0175$, Student's *t* test; Fig. 7*H*,*K*). These data are consistent with our *in vivo* findings, and suggest that hippocampal neurons lacking NCK1 have a reduction in synapse density and an enlargement of the PSDs at remaining synapses.

Since NCK1 was found to localize presynaptically (Fig. 7*A*,*B*, *F*), and previous studies suggest that glutamate release may facilitate synapse formation (Engert and Bonhoeffer, 1999; Kwon and Sabatini, 2011; Quinn et al., 2019), we next wanted to assess whether loss of NCK1 could affect the release of neurotransmitters. To address this, we tested whether neurotransmitter release was perturbed at synapses devoid of NCK1 using synaptophysin-pHluorin (SypHl), a fluorescent sensor for synaptic vesicle exocytosis. SypHl intensity measurements during high-frequency stimulation reveal the size of the readily releasable pool (RRP) of synaptic vesicles at single synapses (Schikorski and Stevens, 2001). The RRP consists of synaptic vesicles which are docked and primed at the membrane and ready for release in response to an action potential. To compare neurotransmitter release at control and NCK1$^{-/-}$ synapses, we transfected control and NCK1$^{-/-}$ cultures with SypHl at DIV 12 and imaged SypHl in response to a high-frequency stimulus train (80 Hz for 1 s) 3 d later. The average synaptic SypHl fluorescence changes per neuron in response to high-frequency stimulation was not significantly different between control and NCK1$^{-/-}$ groups (Control 322.6 ± 11.8 A.U. vs NCK1$^{-/-}$ 299.3 ± 10.9 A.U., $p = 0.1537$, Student's *t* test; Fig. 7*I*,*L*). Together, this result demonstrated that NCK1 is not needed to sustain exocytosis in response to high-frequency stimulation and indicates that synaptic vesicle recycling, docking, and priming is not affected by NCK1 deletion.

Loss of NCK1 results in increased actin recovery in hippocampal dendritic spines after photobleaching

Given that the decrease in spine density was accompanied by a change in the size of the PSD, a region that is regulated by actin-filaments (Kuriu et al., 2006), our data suggest that NCK1 may regulate actin dynamics in the PSD. Therefore, we next turned our focus to whether loss of NCK1 directly affects actin dynamics in the postsynaptic region of dendritic spines. NCK proteins are known to regulate Rho GTPases to affect changes in actin activity either directly through the activation of N-WASP and WAVE which stimulate actin nucleation through the Arp2/3 complex, or through their association with RhoGAP proteins including α2-chimaerin (Eden et al., 2002; Tehrani et al., 2007; Banjade and Rosen, 2014; Okrut et al., 2015). However, no studies have monitored the direct effects on actin dynamics in neurons lacking NCK1. To directly assess whether the effect on spine morphogenesis from loss of NCK1 is directly linked to actin cytoskeleton dynamics, we examined the mobility of GFP-actin in fluorescence recovery after photobleaching (FRAP) experiments. Here, GFP-actin lentiviral particles were transduced in either control or NCK1$^{-/-}$ hippocampal neurons, and FRAP of GFP-actin-labeled dendritic spines was used to assess alterations in actin dynamics. We found that the mobile GFP-actin pool in spines from NCK1$^{-/-}$ neurons was identical to the control and recovered within 60 s of photobleaching (Fig. 8*A*,*B*). Treatment with the actin stabilizing

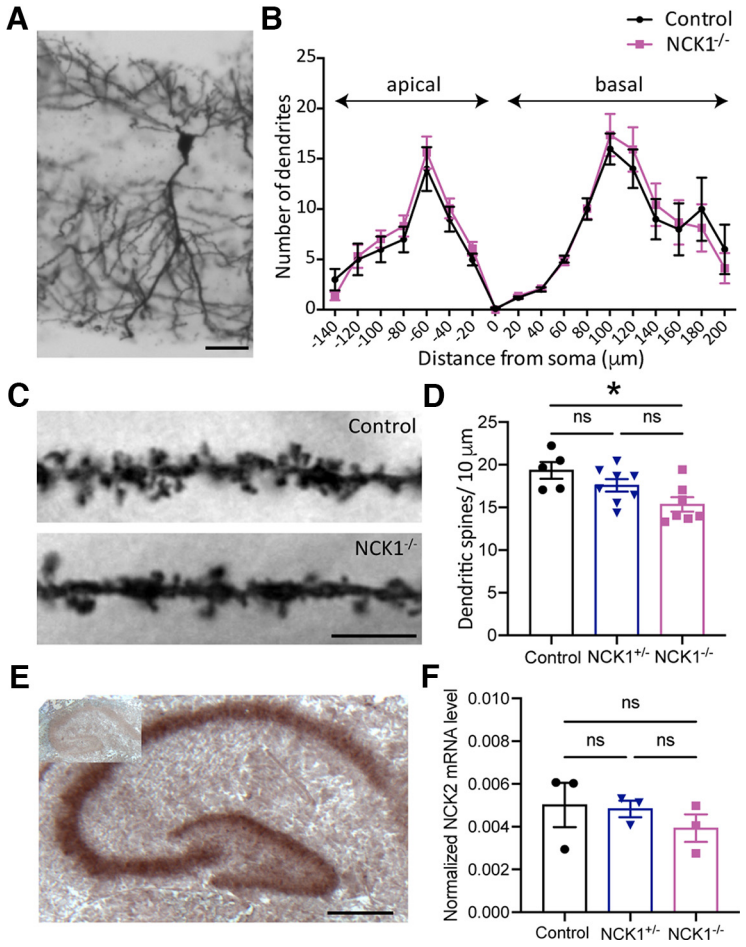

Figure 5. Analysis of dendritic complexity and dendritic spine density in hippocampal neurons of control and NCK1$^{-/-}$ mice. ***A***, Representative image of Golgi stained CA1 hippocampal pyramidal neurons. Scale bar = 40 μm. ***B***, Bidirectional Sholl analysis of control and NCK1$^{-/-}$ CA1 hippocampal pyramidal neurons with apical dendrites being quantified as negative distance from the soma and basal dendrites being quantified as positive distance from the soma. Error bars represent mean ± SEM. ***C***, Representative images of *in vivo* Golgi stained CA1 basal dendrites in control and NCK1$^{-/-}$ mice. Scale bar = 5 μm. ***D***, Quantification of dendritic spine density in the CA1 region in control ($n = 5$), heterozygous (NCK1$^{+/-}$, $n = 8$), and NCK1$^{-/-}$ ($n = 7$) mice. Individual points in the bar graph represents spine average of 20 dendrites per animal. Error bars represent mean ± SEM; ns (not significant), $^{*}p < 0.05$ (one-way ANOVA followed by Tukey's multiple comparisons test). ***E***, NCK2 mRNA expression in postnatal day 7 mouse, insert in upper left panel is the sense control. Scale bar = 500 μm. ***F***, Quantification by qPCR of NCK2 mRNA in the adult hippocampus of control ($n = 3$), NCK1$^{+/-}$ ($n = 3$), and NCK1$^{-/-}$ ($n = 3$) mice. Error bars represent mean ± SEM; ns (not significant), one-way ANOVA followed by Tukey's multiple comparisons test.

compound Jasplakinolide inhibited recovery in control cells (Control 75.98 ± 2.29%, $n = 54$ spines, vs Jasp 2.255 ± 0.507%, $n = 20$ spines and NCK1$^{-/-}$ 80.80 ± 3.180%, $n = 22$ spines, $^{***}p < 0.01$, one-way ANOVA followed by Tukey's *post hoc* test; Fig. 8*C*) demonstrating that the mobility of GFP-actin reflected exchange of new actin filaments. However, actin turnover in neurons lacking NCK1 showed a ~40% faster half-max intensity ($I_{t/2}$) recovery in spines (Control 6853 ± 0.601 $I_{t/2}$ vs NCK1$^{-/-}$ 4.100 ± 1.050 $I_{t/2}$, Student's *t* test, $^{*}p < 0.05$; Fig. 8*D*). This indicates that loss of NCK1 influences normal actin dynamics which is consistent with previous observations in heterologous cells (Garg et al., 2007; Buvall et al., 2013). Since NCK1 controls proteins such as the Arp2/3 complex that favor actin nucleation (Buday et al., 2002), we next examined whether increased actin turnover observed in FRAP is caused by changes in filament polymerization. Using monomeric actin conjugated to rhodamine (Rh-actin), barbed ends in GFP-actin filaments were labeled in live neurons and assessed by imaging (Fig. 8*E*). Quantification of the relative Rh-actin to GFP-actin intensity ratio (A.U.) showed that in NCK1-depleted neurons, Rh-actin was significantly incorporated into polymerizing actin filaments in spines (Control 0.9611 ± 0.033 A.U. vs NCK1$^{-/-}$, 0.7936 ± 0.0323 A.U., $^{***}p < 0.01$, Student's *t* test; Fig. 8*F*). These results demonstrate that loss of NCK1 in hippocampal neurons contributes to altered actin filament dynamics in the postsynaptic density.

Discussion

Our findings indicate that genetic disruption of the adaptor protein NCK1 in male mice results in deficits in memory formation in three hippocampal function-dependent tasks; social recognition (Fig. 1*B*), spontaneous alterations in the Y-maze (Fig. 1*D*), and in learning and remembering the escape platform location in the Morris water maze test (Fig. 2), suggesting NCK1 is as an important regulator of hippocampal function in the adult brain. However, loss of NCK1 did not impact activity levels in any of the tests, nor did it result in impairments in sociability, which suggests that general sensory and motor processes are intact. In fact, the NCK1$^{-/-}$ mice have no apparent olfactory, visual, or motor deficits (Fawcett et al., 2007; Diab et al., 2020), suggesting that sensory and motor neuronal circuitry is functional in these mutant mice. Additionally, no differences were found in brain size or shape between NCK1$^{-/-}$ mice and control mice. Correspondingly, no differences in embryonic neuronal proliferation or in hippocampal development were found (Fig. 4), further suggesting that basic neuronal development is not impaired in the NCK1$^{-/-}$ mice. Together, these data suggest that the learning and memory impairment may be because of deficiencies in postnatal hippocampal function.

Interestingly, we found sex-dependent differences in all memory related behavioral tasks but not in sociability or overall activity (Figs. 1, 2), consistent with our previous studies in which we identified that NCK1 plays a role in sex-dependent differences in context-dependent avoidant behaviors (Diab et al., 2020). In both the social recognition task and Y-maze, female control and NCK1$^{-/-}$ mice performed similarly to male NCK1$^{-/-}$ mice, suggesting that the female mice were unable to learn these tasks regardless of genotype (Fig. 1*B*,*D*). Mouse strain and sex-dependent differences in short-term memory tasks have been previously reported suggesting that male rodents have an advantage in working memory tasks (Jonasson, 2005). Importantly, given that female control mice underperformed in our Y-maze and social recognition protocols, future studies should develop short-term and working memory protocols that clearly demonstrate the female control mice's ability to perform in the task at which point the effect of NCK1 deficiency on short-term and working memory in female mice can be better assessed. We also report sex-dependent differences in spatial learning in the Morris water maze (Fig. 2), with male mice

lacking NCK1 having impairments in both memory acquisition and reversal learning (Fig. 2*A*,*C*,*F*), while the female mice lacking NCK1 performed similar to their littermate controls in memory acquisition, but failed in the reversal phase of the task (Fig. 2*B*,*D*,*G*,*H*), suggesting a decreased cognitive flexibility in the female NCK1$^{-/-}$ mice. Interestingly, C57BL6/N mice with hippocampal lesions and women with unilateral hippocampal sclerosis display impairment in reversal learning (Kleinknecht et al., 2012; Vilà-Balló et al., 2017) suggesting that damaged hippocampal function can result in impairments in reversal learning. One explanation for the observed sex difference in the NCK1$^{-/-}$ mice may be because of a difference in escape strategies used by male and female mice (Mizuno and Giese, 2010), with NCK1 deficiency more greatly impairing the escape strategy used by male mice. Additionally, it is becoming increasingly clear that sex-dependent differences in brain function and behavior are reflective of differences in synaptic signaling mechanisms (Mizuno and Giese, 2010). Therefore, future work exploring differences in male and female synaptic signaling pathways, and NCK1's role in those pathways, will lead to greater insight into molecular signaling pathways important for memory acquisition, reversal learning, and cognitive flexibility.

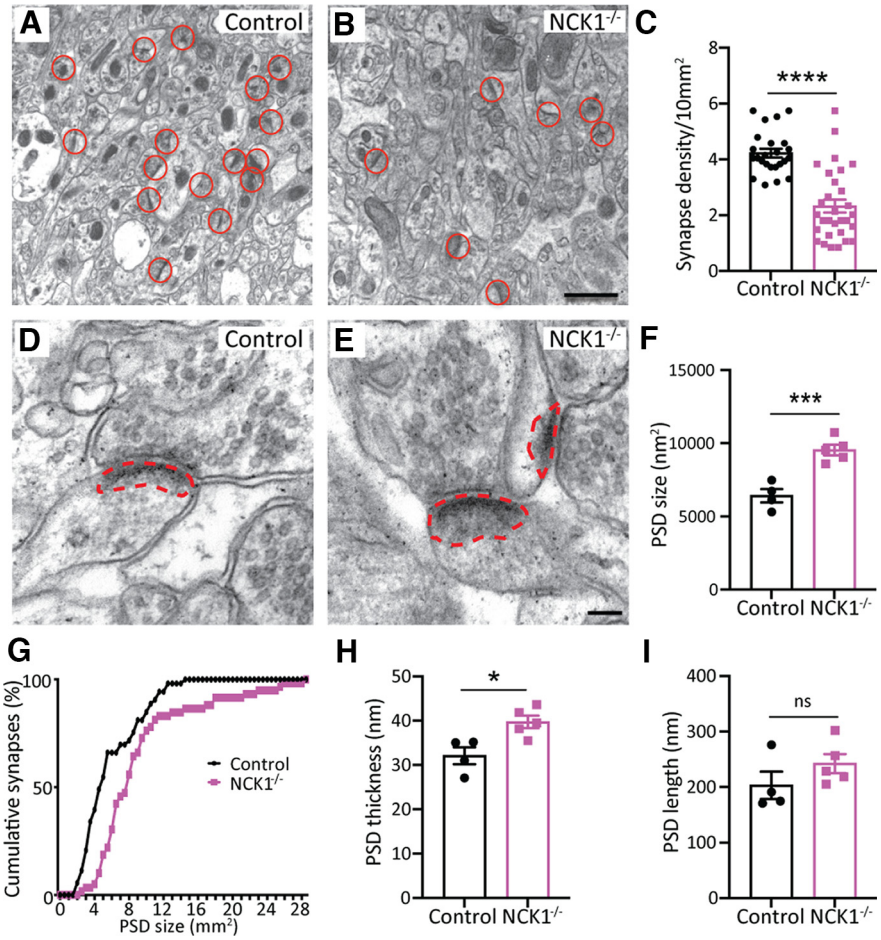

Figure 6. Analysis synapse density and postsynaptic density morphology in the hippocampi of control and NCK1$^{-/-}$ mice. ***A***, ***B***, Representative images of transmission electron micrographs (TEM) from the hippocampus of control and NCK1$^{-/-}$ mice. Red circles outline synapses. Scale bar = 1 μm. ***C***, Quantification of hippocampal synapse density per 10 μm^2 acquired by TEM. Error bars represent mean ± SEM; ****$p < 0.0001$ (Student's *t* test). ***D***, ***E***, Identification of a hippocampal synapse acquired by TEM. Broken red line outlines the postsynaptic density (PSD). Scale bar = 100 nm. ***F***, Quantification of PSD size. Error bars represent mean ± SEM; ***$p < 0.001$ (Student's *t* test). ***G***, Cumulative percentage of PSD size in control and NCK1$^{-/-}$ synapses. ***H***, Quantification of PSD thickness. Error bars represent mean ± SEM; *$p < 0.05$ (Student's *t* test). ***I***, Quantification of PSD length. Error bars represent mean ± SEM; ns $p > 0.05$ (Student's *t* test).

Analysis of NCK1 expression revealed that NCK1 is present in all postmitotic neurons in the hippocampus, including interneurons, and in ~15% of astrocytes, but not in microglia, oligodendrocytes, nor in the progenitor cell layer of the dentate gyrus (Fig. 3). Therefore, NCK1 likely functions in mature excitatory neurons, inhibitory interneurons, and in a subpopulation of astrocytes and is not involved in the proliferation or migration of these cell types. Consistent with our data, a recent report showed that NCK2, but not NCK1, affects cellular proliferation (Jacquet et al., 2018).

Mice lacking NCK1 showed no overall changes in the branching of either apical or basal dendritic arbors in CA1 pyramidal neurons. (Figs. 5*A*,*B*, 7*C*). In contrast, NCK1$^{-/-}$ mice showed decreased dendritic spine density in both Golgi-stained sections and in EM analysis (Figs. 5*C*,*D*, 6*C*), as well as reduced Homer1 density (Fig. 7*H*,*J*), suggesting that NCK1 is essential for proper spine development. In addition to the reduced spine density, we report that NCK1 deficiency resulted in an increase in PSD size and thickness in our EM analysis (Fig. 6*D*–*H*) that was supported by an increased Homer staining intensity in individual spines in our dissociated cultures (Fig. 7*H*,*K*). The increased PSD size is consistent with activity-induced recruitment of postsynaptic proteins (Dosemeci et al., 2001, 2016; Sheng and Kim, 2011; Meyer et al., 2014), and thus potentially more dynamic synapses. The increased PSD size and thickness may be a direct effect of NCK1 deficiency, consistent with our finding that NCK1 is associated with the postsynaptic density (Fig. 7*B*), or an indirect homeostatic effect whereby the strength at remaining synapses is increased to compensate for lower densities of glutamatergic synapses.

Our FRAP and rhodamine actin incorporation studies suggest that NCK1 deficiency leads to an increased rate of actin turnover and polymerization in dendritic spines of NCK1-deficient neurons (Fig. 8). Therefore, the increased actin turnover and polymerization rate may destabilize spines or prevent their formation through altered actin treadmilling, which in turn may trigger spatial and or functional modulation of actin regulators important for dendritic spine life cycle regulation (Fig. 8*G*). Indeed, actin cytoskeletal polymerization, depolymerization and branching is critical for dendritic spine and memory formation, and has been shown to be regulated by the small GTPases Rac1, Cdc42, Rho GTPases, and their downstream effectors such as Arp2/3 and WAVE1 (Woolfrey and Srivastava, 2016; Basu and Lamprecht, 2018). Interestingly, loss of WAVE1 results in reductions in dendritic spine density and in learning and memory impairments in the Morris water maze (Soderling et al., 2007), similar to what we find in NCK1-deficient mice. Indeed, NCK1 has been shown to interact with Rac1 to activate WAVE1 and influence actin nucleation (Eden et al., 2002). However, if this is

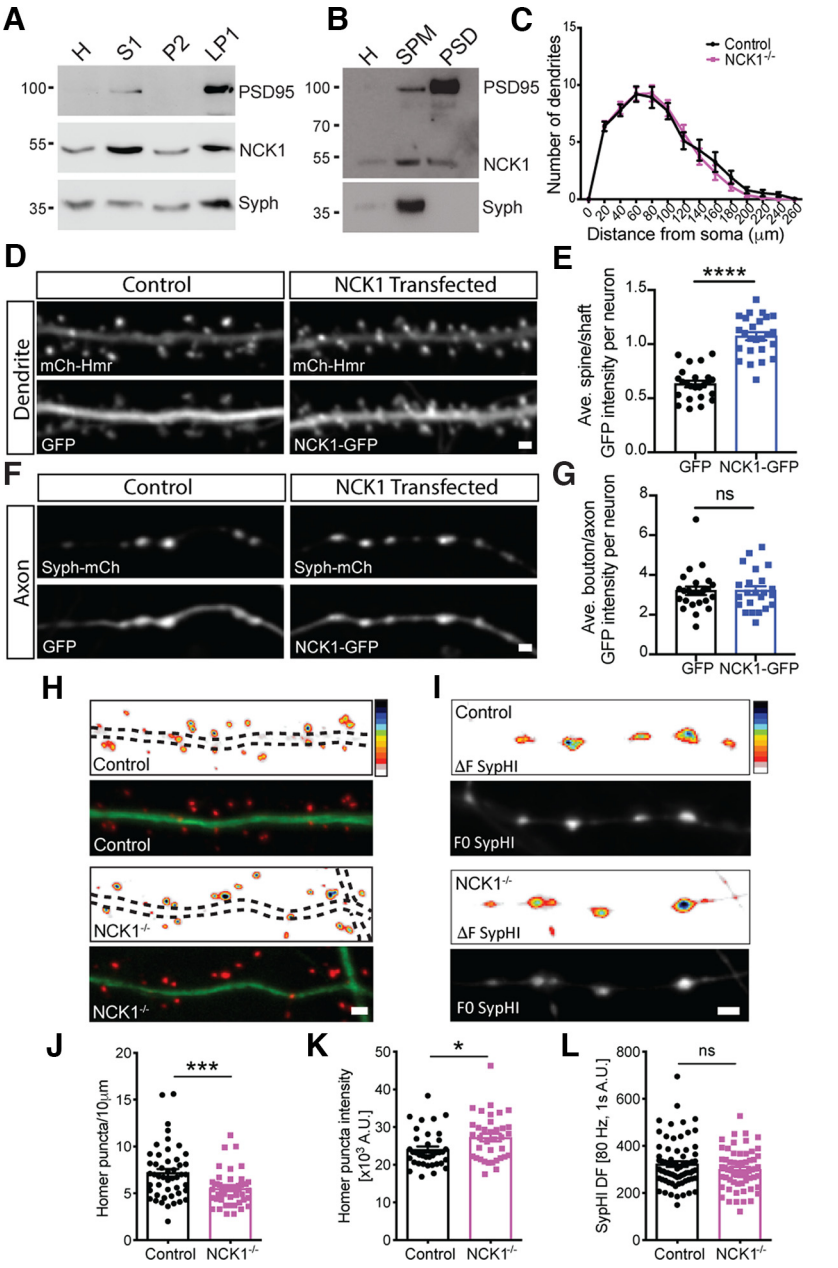

Figure 7. Synaptic localization of NCK1 and effects of NCK1 loss on dendrite arborization. ***A***, Enrichment of endogenous NCK1 in adult rat brain preparations obtained by ultracentrifugation. 10 μg per well of Homogenate (H), supernatant (S1), pellet (P2), and synaptosomal membrane (LP1) was analyzed by SDS-PAGE. Proteins were detected by immunoblotting using the indicated antibodies. Synaptophysin (Syph). ***B***, Crude synaptosomal membranes (LP1) were further treated with Triton X-100 to generate the post-synaptic density (PSD) fractions. Total homogenates (10 μg) were compared with 30 μg of synaptic plasma membrane (SPM) and PSD fractions. Proteins were detected with the indicated antibodies. ***C***, Sholl analysis of control and NCK1$^{-/-}$ cultured hippocampal neurons. Error bars represent mean ± SEM. ***D***, Example micrographs of dissociated rat hippocampal neurons co-expressing mcherry-Homer1b (mCh-Hmr) to label spines/dendrites and either GFP (Control) or NCK1-GFP. Scale bar = 1 μm. ***E***, NCK1-GFP is enriched in dendritic spines compared with cytosolic GFP. Quantification of average spine/shaft GFP intensity per neuron in cells expression cytosolic GFP (Control) or NCK1-GFP. $n = 24$ neurons (386 spines) for GFP group and 25 neurons (467 spines) for NCK1-GFP group. Error bars represent mean ± SEM; ****$p < 0.0001$ (Student's t test). ***F***, Example micrographs of dissociated rat hippocampal neurons co-expressing Synaptophysin-mCherry (Syph-mCh) to label presynaptic boutons/axons and either GFP (Control) or NCK1-GFP. Scale bar = 1 μm. ***G***, NCK1-GFP is not enriched at presynaptic sites compared with cytosolic GFP. Quantification of average bouton/axon GFP intensity per neuron in cells expression cytosolic GFP (Control) or NCK1-GFP. $n = 23$ neurons (333 boutons) for GFP group and 22 neurons (248 boutons) for NCK1-GFP group. Error bars represent mean ± SEM; ns (not significant) $p > 0.05$ (Student's t test). ***H***, Cultured neurons from control and NCK1$^{-/-}$ mice immunostained for endogenous Homer (red) and MAP2 (green) and heat map images of homer fluorescence intensity along the dendrites. The pseudo color bar indicates black as the highest level of fluorescence intensity and white as the lowest. Scale bar = 1 μm. ***I***, Control and NCK1$^{-/-}$ axons transfected with synaptophysin-pHluorin (SypHI). Gray-scale images show basal SypHI fluorescence and ΔF images show SypHI fluorescence increases during high frequency electrical stimulation (80 Hz, 1 s). The pseudo color bar indicates black as the highest level of fluorescence intensity and white as the lowest. Scale bar = 1 μm. ***J***, Quantification of homer puncta along dendrites. Error bars represent mean ± SEM; ***$p < 0.001$ (Student's t test). ***K***, Quantification of homer puncta intensity (arbitrary units, A.U.). Error bars represent mean ± SEM; *$p < 0.05$ (Student's t test). ***L***, Quantification of changes in SypHI fluorescence intensity (A.U.) after a high-frequency stimulus train (80 Hz for 1 s, ΔF). Error bars represent mean ± SEM; ns (not significant) $p > 0.05$ (Student's t test).

occurring in dendritic spines remains to be addressed. Together, these data suggest a novel function for NCK1 in regulating actin stability in dendritic spines, and this stabilization may be important for the formation and/or maintenance of synapses in the adult hippocampus. Future work to directly test which region in NCK1 and which interacting proteins associate with NCK1 in neurons to directly couple to actin dynamics will be important to further define this pathway.

Upstream of NCK1, multiple signaling pathways converge on actin-cytoskeletal rearrangement to regulate activity-dependent spine morphogenesis, maintenance, and elimination (Caroni et al., 2012; Basu and Lamprecht, 2018) Indeed, the netrin-1 receptor DCC, a known upstream recruiter of NCK1 (Li et al., 2002), has been shown to be critical for synaptogenesis, synapse maturation, and memory formation in the mammalian brain (Goldman et al., 2013; Horn et al., 2013; Glasgow et al., 2018; E.W. Wong et al., 2019). Interestingly, aged mice that have conditional deletion of DCC or netrin-1 in the forebrain develop deficits in spatial and recognition memory similar to what is seen in the NCK1-mutant mice (Horn et al., 2013; E.W. Wong et al., 2019). Recent work suggests that netrin-1 functions in hippocampal dendritic spine maturation by promoting GluA1-containing AMPA receptor insertion into the PSD through a DCC-mediated mechanism (Glasgow et al., 2018). NCK1 may be playing a role downstream of DCC to influence actin dynamics in the spine as actin regulation has been implicated in postsynaptic receptor anchoring and trafficking (Cingolani and Goda, 2008). However, the role of actin cytoskeletal reorganization in the DCC-mediate receptor insertion remains to be addressed, and this will be important as a role for NCK proteins in DCC-meditated actin rearrangement in axon guidance and growth cone morphology has been established (Shekarabi et al., 2005; Lane et al., 2015). In addition, NCK proteins have been linked to Eph and B-type ephrin dependent signaling, both of which have been implicated in synapse formation (Stein et al., 1998; Hruska and

Dalva, 2012). Interestingly, our attempts to restore dendritic spines in NCK1-deficient neurons by overexpression were unsuccessful. Whether this reflects a technical aspect of our experimental design, or developmental timing, including whether upstream receptor complexes fail to engage with re-expressed NCK1 remain to be determined. In this context, it will be important to further characterize which receptor complex NCK1 signals through and at what developmental timeline. Further, our finding that NCK2 is present in the hippocampus (Fig. 5*E*) and its mRNA is present in the NCK1 mutant background (Fig. 5*F*), will necessitate more refined genetic strategies to help determine which signaling complexes function *in vivo* to modulate learning and memory behaviors and neuronal morphologies.

NCK1 has also been shown to function upstream of Rho-GTPases. The Rho-GTPases, RhoA, Rac1, and Cdc42, are well-known regulators of the actin cytoskeleton that have been shown to influence dendritic spine formation, maintenance, and elimination (Tada and Sheng, 2006). Interestingly, whereas RhoA activation inhibits spine morphogenesis and promotes spine elimination, Cdc42 and Rac1 activation promotes spine formation (Tashiro et al., 2000; Tashiro and Yuste, 2004). Indeed, in embryonic and dermal fibroblasts NCK1 has been shown to be involved in Rac1 and Cdc42 activity (Li et al., 2002; Guan et al., 2009), but not in RhoA activity (Guan et al., 2009). However, in podocytes, proteasomal degradation of NCK1 has been shown to regulate actin dynamics through RhoA activation (Buvall et al., 2013), suggesting that NCK1 may play a cell-type and context dependent role in actin regulation. In neurons, loss of NCK1 may be impairing Rac1 and/or Cdc42 activation and their association with upstream and downstream modulators of the actin cytoskeleton and thus resulting in the decreased spine density observed in the NCK1$^{-/-}$ mice by preventing dendritic spine formation. Similarly to the NCK1 mutant mice, *in vivo* conditional deletion of Rac1 or Cdc42 in the forebrain postnatally results in decreased spine density in the CA1 region of the hippocampus, and deficits in spatial memory and learning in the Morris water maze (Haditsch et al., 2009; Kim et al., 2014). Future work looking at Rho-GTPase activity in NCK1-deficient neurons will provide insight into NCK1's role in Rho-GTPase activation in dendritic spines. This is critical, as NCK proteins have been linked with α2-chimaerin and PAK dependent signaling to affect Rho-GTPase activity (Sells et al., 1997; Wegmeyer et al., 2007). Whether Rho-GTPase activity is linked to either NCK1 or NCK2 remains to be established, and whether there is tissue/cell-type specific modulation also remains unknown. Further, whether NCK proteins directly affect synaptic plasticity *in vivo* remains to be tested, as the association between PAK3 and NCK2 has been shown to directly regulate synaptic plasticity independent of spine morphogenesis, and recently Nck2 has been shown to associate with NMDA subunits to affect GluN2B-mediated neurotransmission (Thévenot et al., 2011; Levy et al., 2018). Nonetheless, it is important to understand how NCK1 regulates actin dynamics in the PSD as the PSD is a region important for maintaining appropriate scaffolding proteins that link F-actin with membrane receptors critical for neuronal signaling, synapse formation, and maintenance. Understanding the molecular pathways involved in regulating the PSD is critical for allowing us to understand how changes in this region alter neuronal function, memory, and behavior.

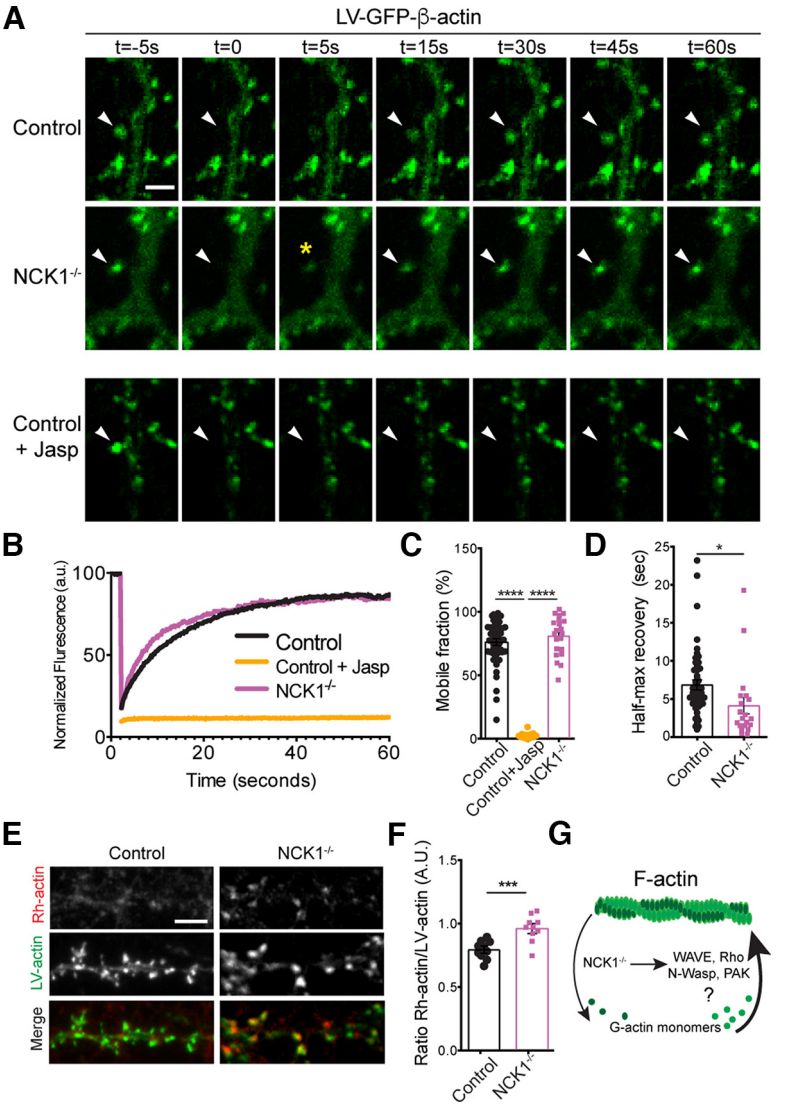

Figure 8. Destabilized actin turnover in NCK1-deficient neurons. ***A***, Time lapse images show GFP-actin (LV-GFP-β-actin) turnover without or with Jasplakinolide (Jasp; 30 min pretreatment, 1 μM) at the indicated time points in control and NCK1$^{-/-}$ neurons. Arrowheads point to bleached spines. Asterisks indicate enhanced kinetics of GFP-actin at $t = 5$ s postbleaching in NCK1-deficient cells. Scale bar = 5 μm. ***B***, Normalized data fit into single exponential decay curves of fluorescence recovery (*y*-axis) plotted against time (*x*-axis) after photobleaching. ***C***, Quantification of GFP-actin mobility in dendritic spines after photobleaching. Error bars represent mean ± SEM; ****$p < 0.0001$ (one-way ANOVA followed by Tukey's multiple comparisons test). ***D***, Quantification of half-maximum recovery (in seconds) in dendritic spines after photobleaching. Error bars represent mean ± SEM; *$p < 0.05$ (Student's *t* test). ***E***, Visualization of monomeric rhodamine (Rh)-actin incorporated at barbed ends in filaments visualized with GFP-actin. ***F***, Bar graphs show quantification of relative intensity ratio (A.U.) of Rh-actin to GFP-actin in dendritic spines. Error bars represent mean ± SEM; ***$p < 0.001$ (Student's *t* test). ***G***, Schematic summarizing the results of Figure 7. Loss of NCK1 in hippocampal neurons results in increased incorporation of globular (G)-actin monomers into filamentous (F)-actin and an imbalance in actin turnover in dendritic spines.

Closer examination of the role of NCK *in vivo*, actin, and their influence on the PSD will be important in future studies.

In summary, here we demonstrate that NCK1 is necessary for social recognition, working memory capacity, and spatial learning in a sex specific manner. These effects may be independent of developmental influences, as loss of NCK1 has no effect on progenitor cell proliferation or migration in the hippocampus. The behavioral defects are likely linked to impaired actin dynamics within the dendritic spines of hippocampal neurons. Finally, our data demonstrate that NCK1 plays a role in cognition, specifically in learning and memory, perhaps by modulating actin turnover within dendritic spines to modulate accumulation of scaffolding proteins in the PSD. Together, our data suggest that NCK1 is an important regulator of actin stability in dendritic spines and plays a role in memory formation.

References

Bailey CH, Kandel ER, Harris KM (2015) Structural components of synaptic plasticity and memory consolidation. Cold Spring Harb Perspect Biol 7: a021758.

Banjade S, Rosen MK (2014) Phase transitions of multivalent proteins can promote clustering of membrane receptors. Elife 3:e04123.

Basu S, Lamprecht R (2018) The role of actin cytoskeleton in dendritic spines in the maintenance of long-term memory. Front Mol Neurosci 11:1795.

Bladt F, Aippersbach E, Gelkop S, Strasser GA, Nash P, Tafuri A, Gertler FB, Pawson T (2003) The Murine Nck SH2/SH3 adaptors are important for the development of mesoderm-derived embryonic structures and for regulating the cellular actin network. Mol Cell Biol 23:4586–4597.

Blanpied TA, Kerr JM, Ehlers MD (2008) Structural plasticity with preserved topology in the postsynaptic protein network. Proc Natl Acad Sci U S A 105:12587–12592.

Bokoch GM, Wang Y, Bohl BP, Sells MA, Quilliam LA, Knaus UG (1996) Interaction of the Nck adapter protein with p21-activated kinase (PAK1). J Biol Chem 271:25746–25749.

Buday L, Wunderlich L, Tamás P (2002) The Nck family of adapter proteins: regulators of actin cytoskeleton. Cell Signal 14:723–731.

Buvall L, Rashmi P, Lopez-Rivera E, Andreeva S, Weins A, Wallentin H, Greka A, Mundel P (2013) Proteasomal degradation of Nck1 but not Nck2 regulates RhoA activation and actin dynamics. Nat Commun 4:2863.

Caroni P, Donato F, Muller D (2012) Structural plasticity upon learning: regulation and functions. Nat Rev Neurosci 13:478–490.

Chaki SP, Barhoumi R, Berginski ME, Sreenivasappa H, Trache A, Gomez SM, Rivera GM (2013) Nck enables directional cell migration through the coordination of polarized membrane protrusion with adhesion dynamics. J Cell Sci 126:1637–1649.

Chazeau A, Giannone G (2016) Organization and dynamics of the actin cytoskeleton during dendritic spine morphological remodeling. Cell Mol Life Sci 73:3053–3073.

Chen M, She H, Davis EM, Spicer CM, Kim L, Ren R, Beau MML, Li W (1998) Identification of Nck family genes, chromosomal localization, expression, and signaling specificity. J Biol Chem 273:25171–25178.

Cingolani LA, Goda Y (2008) Actin in action: the interplay between the actin cytoskeleton and synaptic efficacy. Nat Rev Neurosci 9:344–356.

Civiero L, Greggio E (2018) PAKs in the brain: function and dysfunction. Biochim Biophys Acta Mol Basis Dis 1864:444–453.

Clouthier DL, Harris CN, Harris RA, Martin CE, Puri MC, Jones N (2015) Requisite role for Nck adaptors in cardiovascular development, endothelial-to-mesenchymal transition, and directed cell migration. Mol Cell Biol 35:1573–1587.

Cowan CA, Henkemeyer M (2001) The SH2/SH3 adaptor Grb4 transduces B-ephrin reverse signals. Nature 413:174–179.

Diab A, Qi J, Shahin I, Milligan C, Fawcett JP (2020) NCK1 regulates amygdala activity to control context-dependent stress responses and anxiety in male mice. Neuroscience 448:107–125.

Dines M, Lamprecht R (2015) The pole of ephs and ephrins in memory formation. Int J Neuropsychopharmacol 19:pyv106.

Dosemeci A, Tao-Cheng J-H, Vinade L, Winters CA, Pozzo-Miller L, Reese TS (2001) Glutamate-induced transient modification of the postsynaptic density. Proc Natl Acad Sci U S A 98:10428–10432.

Dosemeci A, Weinberg RJ, Reese TS, Tao-Cheng JH (2016) The postsynaptic density: there is more than meets the eye. Front Synaptic Neurosci 8:23.

Dubrac A, Künzel SE, Künzel SH, Li J, Chandran RR, Martin K, Greif DM, Adams RH, Eichmann A (2018) NCK-dependent pericyte migration promotes pathological neovascularization in ischemic retinopathy. Nat Commun 9:3463.

Eden S, Rohatgi R, Podtelejnikov AV, Mann M, Kirschner MW (2002) Mechanism of regulation of WAVE1-induced actin nucleation by Rac1 and Nck. Nature 418:790–793.

Engert F, Bonhoeffer T (1999) Dendritic spine changes associated with hippocampal long-term synaptic plasticity. Nature 399:66–70.

Fawcett JP, Georgiou J, Ruston J, Bladt F, Sherman A, Warner N, Saab BJ, Scott R, Roder JC, Pawson T (2007) Nck adaptor proteins control the organization of neuronal circuits important for walking. Proc Natl Acad Sci U S A 104:20973–20978.

Feder TJ, Brust-Mascher I, Slattery JP, Baird B, Webb WW (1996) Constrained diffusion or immobile fraction on cell surfaces: a new interpretation. Biophys J 70:2767–2773.

Fiala JC, Spacek J, Harris KM (2002) Dendritic spine pathology: cause or consequence of neurological disorders? Brain Res Brain Res Rev 39:29–54.

Fonseca R, Vabulas RM, Hartl FU, Bonhoeffer T, Nägerl UV (2006) A balance of protein synthesis and proteasome-dependent degradation determines the maintenance of LTP. Neuron 52:239–245.

Garg P, Verma R, Nihalani D, Johnstone DB, Holzman LB (2007) Neph1 cooperates with nephrin to transduce a signal that induces actin polymerization. Mol Cell Biol 27:8698–8712.

Glasgow SD, Labrecque S, Beamish IV, Aufmkolk S, Gibon J, Han D, Harris SN, Dufresne P, Wiseman PW, McKinney RA, Séguéla P, De Koninck P, Ruthazer ES, Kennedy TE (2018) Activity-dependent netrin-1 secretion drives synaptic insertion of GluA1-containing AMPA receptors in the hippocampus. Cell Rep 25:168–182.e6.

Goldman JS, Ashour MA, Magdesian MH, Tritsch NX, Harris SN, Christofi N, Chemali R, Stern YE, Thompson-Steckel G, Gris P, Glasgow SD, Grutter P, Bouchard J-F, Ruthazer ES, Stellwagen D, Kennedy TE (2013) Netrin-1 promotes excitatory synaptogenesis between cortical neurons by initiating synapse assembly. J Neurosci 33:17278–17289.

Grove M, Demyanenko G, Echarri A, Zipfel PA, Quiroz ME, Rodriguiz RM, Playford M, Martensen SA, Robinson MR, Wetsel WC, Maness PF, Pendergast AM (2004) ABI2-deficient mice exhibit defective cell migration, aberrant dendritic spine morphogenesis, and deficits in learning and memory. Mol Cell Biol 24:10905–10922.

Gu J, Lee CW, Fan Y, Komlos D, Tang X, Sun C, Yu K, Hartzell HC, Chen G, Bamburg JR, Zheng JQ (2010) ADF/cofilin-mediated actin dynamics regulate AMPA receptor trafficking during synaptic plasticity. Nat Neurosci 13:1208–1215.

Guan S, Fan J, Han A, Chen M, Woodley DT, Li W (2009) Non-compensating roles between Nckalpha and Nckbeta in PDGF-BB signaling to promote human dermal fibroblast migration. J Invest Dermatol 129:1909–1920.

Haditsch U, Leone DP, Farinelli M, Chrostek-Grashoff A, Brakebusch C, Mansuy IM, McConnell SK, Palmer TD (2009) A central role for the small GTPase Rac1 in hippocampal plasticity and spatial learning and memory. Mol Cell Neurosci 41:409–419.

Hayashi MK, Tang C, Verpelli C, Narayanan R, Stearns MH, Xu R-M, Li H, Sala C, Hayashi Y (2009) The postsynaptic density proteins Homer and Shank form a polymeric network structure. Cell 137:159–171.

Hayashi-Takagi A, Yagishita S, Nakamura M, Shirai F, Wu YI, Loshbaugh AL, Kuhlman B, Hahn KM, Kasai H (2015) Labelling and optical erasure of synaptic memory traces in the motor cortex. Nature 525:333–338.

Herms J, Dorostkar MM (2016) Dendritic spine pathology in neurodegenerative diseases. Annu Rev Pathol 11:221–250.

Holland SJ, Gale NW, Gish GD, Roth RA, Songyang Z, Cantley LC, Henkemeyer M, Yancopoulos GD, Pawson T (1997) Juxtamembrane tyrosine residues couple the Eph family receptor EphB2/Nuk to specific SH2 domain proteins in neuronal cells. EMBO J 16:3877–3888.

Horn KE, Glasgow SD, Gobert D, Bull S-J, Luk T, Girgis J, Tremblay M-E, McEachern D, Bouchard J-F, Haber M, Hamel E, Krimpenfort P, Murai KK, Berns A, Doucet G, Chapman CA, Ruthazer ES, Kennedy TE (2013)

DCC expression by neurons regulates synaptic plasticity in the adult brain. Cell Rep 3:173–185.
Hruska M, Dalva MB (2012) Ephrin regulation of synapse formation, function and plasticity. Mol Cell Neurosci 50:35–44.
Jacquet K, Banerjee SL, Chartier FJM, Elowe S, Bisson N (2018) Proteomic analysis of NCK1/2 adaptors uncovers paralog-specific interactions that reveal a new role for NCK2 in cell abscission during cytokinesis. Mol Cell Proteomics 17:1979–1990.
Jonasson Z (2005) Meta-analysis of sex differences in rodent models of learning and memory: a review of behavioral and biological data. Neurosci Biobehav Rev 28:811–825.
Karpova A, Mikhaylova M, Thomas U, Knöpfel T, Behnisch T (2006) Involvement of protein synthesis and degradation in long-term potentiation of Schaffer collateral CA1 synapses. J Neurosci 26:4949–4955.
Kelly ML, Chernoff J (2012) Mouse models of PAK function. Cell Logist 2:84–88.
Kim IH, Racz B, Wang H, Burianek L, Weinberg R, Yasuda R, Wetsel WC, Soderling SH (2013) Disruption of Arp2/3 results in asymmetric structural plasticity of dendritic spines and progressive synaptic and behavioral abnormalities. J Neurosci 33:6081–6092.
Kim IH, Wang H, Soderling SH, Yasuda R (2014) Loss of Cdc42 leads to defects in synaptic plasticity and remote memory recall. Elife 3:e02839.
Kleinknecht K, Bedenk B, Kaltwasser S, Grünecker B, Yen YC, Czisch M, Wotjak C (2012) Hippocampus-dependent place learning enables spatial flexibility in C57BL6/N mice. Front Behav Neurosci 6:87.
Kraeuter AK, Guest PC, Sarnyai Z (2019) The Y-maze for assessment of spatial working and reference memory in mice. Methods Mol Biol 1916:105–111.
Kuriu T, Inoue A, Bito H, Sobue K, Okabe S (2006) Differential control of postsynaptic density scaffolds via actin-dependent and -independent mechanisms. J Neurosci 26:7693–7706.
Kwon H-B, Sabatini BL (2011) Glutamate induces de novo growth of functional spines in developing cortex. Nature 474:100–104.
Lalonde R (2002) The neurobiological basis of spontaneous alternation. Neurosci Biobehav Rev 26:91–104.
Lamprecht R, LeDoux J (2004) Structural plasticity and memory. Nat Rev Neurosci 5:45–54.
Lane C, Qi J, Fawcett JP (2015) NCK is critical for the development of deleted in colorectal cancer (DCC) sensitive spinal circuits. J Neurochem 134:1008–1014.
Levy AD, Xiao X, Shaw JE, Sudarsana Devi SP, Katrancha SM, Bennett AM, Greer CA, Howe JR, Machida K, Koleske AJ (2018) Noonan syndrome-associated SHP2 dephosphorylates GluN2B to regulate NMDA receptor function. Cell Rep 24:1523–1535.
Li X, Meriane M, Triki I, Shekarabi M, Kennedy TE, Larose L, Lamarche-Vane N (2002) The adaptor protein Nck-1 couples the netrin-1 receptor DCC (deleted in colorectal cancer) to the activation of the small GTPase Rac1 through an atypical mechanism. J Biol Chem 277:37788–37797.
Lippincott-Schwartz J, Presley JF, Zaal KJM, Hirschberg K, Miller CD, Ellenberg J (1998) Monitoring the dynamics and mobility of membrane proteins tagged with green fluorescent protein. Methods Cell Biol 58:261–281.
Lu KH, Keppler S, Leithäuser F, Mattfeldt T, Castello A, Kostezka U, Küblbeck G, Schmitt S, Klevenz A, Prokosch S, Pougialis G, Pawson T, Batista F, Tafuri A, Arnold B (2015) Nck adaptor proteins modulate differentiation and effector function of T cells. J Leukoc Biol 98:301–311.
Mantzur L, Joels G, Lamprecht R (2009) Actin polymerization in lateral amygdala is essential for fear memory formation. Neurobiol Learn Mem 91:85–88.
Martínez-Cerdeño V (2017) Dendrite and spine modifications in autism and related neurodevelopmental disorders in patients and animal models. Dev Neurobiol 77:393–404.
Matz J, Gilyan A, Kolar A, McCarvill T, Krueger SR (2010) Rapid structural alterations of the active zone lead to sustained changes in neurotransmitter release. Proc Natl Acad Sci U S A 107:8836–8841.
Meng J, Meng Y, Hanna A, Janus C, Jia Z (2005) Abnormal long-lasting synaptic plasticity and cognition in mice lacking the mental retardation gene Pak3. J Neurosci 25:6641–6650.
Meyer D, Bonhoeffer T, Scheuss V (2014) Balance and stability of synaptic structures during synaptic plasticity. Neuron 82:430–443.
Minerbi A, Kahana R, Goldfeld L, Kaufman M, Marom S, Ziv NE (2009) Long-term relationships between synaptic tenacity, synaptic remodeling, and network activity. PLoS Biol 7:e1000136.
Mizuno K, Giese KP (2010) Towards a molecular understanding of sex differences in memory formation. Trends Neurosci 33:285–291.
Moy SS, Nadler JJ, Perez A, Barbaro RP, Johns JM, Magnuson TR, Piven J, Crawley JN (2004) Sociability and preference for social novelty in five inbred strains: an approach to assess autistic-like behavior in mice. Genes Brain Behav 3:287–302.
Nagura H, Ishikawa Y, Kobayashi K, Takao K, Tanaka T, Nishikawa K, Tamura H, Shiosaka S, Suzuki H, Miyakawa T, Fujiyoshi Y, Doi T (2012) Impaired synaptic clustering of postsynaptic density proteins and altered signal transmission in hippocampal neurons, and disrupted learning behavior in PDZ1 and PDZ2 ligand binding-deficient PSD-95 knockin mice. Mol Brain 5:43.
Nelson BS, Witty CF, Williamson EA, Daniel JM (2012) A role for hippocampal actin rearrangement in object placement memory in female rats. Neurobiol Learn Mem 98:284–290.
Okrut J, Prakash S, Wu Q, Kelly MJS, Taunton J (2015) Allosteric N-WASP activation by an inter-SH3 domain linker in Nck. Proc Natl Acad Sci U S A 112:E6436–E6445.
Pilpel Y, Segal M (2005) Rapid WAVE dynamics in dendritic spines of cultured hippocampal neurons is mediated by actin polymerization. J Neurochem 95:1401–1410.
Quinn DP, Kolar A, Harris SA, Wigerius M, Fawcett JP, Krueger SR (2019) The stability of glutamatergic synapses is independent of activity level, but predicted by synapse size. Front Cell Neurosci 13:291.
Rehberg K, Bergado-Acosta JR, Koch JC, Stork O (2010) Disruption of fear memory consolidation and reconsolidation by actin filament arrest in the basolateral amygdala. Neurobiol Learn Mem 94:117–126.
Richter K, Wolf G, Engelmann M (2005) Social recognition memory requires two stages of protein synthesis in mice. Learn Mem 12:407–413.
Rohatgi R, Nollau P, Ho H-YH, Kirschner MW, Mayer BJ (2001) Nck and phosphatidylinositol 4,5-bisphosphate synergistically activate actin polymerization through the N-WASP-Arp2/3 pathway. J Biol Chem 276:26448–26452.
Rust MB, Gurniak CB, Renner M, Vara H, Morando L, Görlich A, Sassoè-Pognetto M, Banchaabouchi MA, Giustetto M, Triller A, Choquet D, Witke W (2010) Learning, AMPA receptor mobility and synaptic plasticity depend on n-cofilin-mediated actin dynamics. EMBO J 29:1889–1902.
Sala C, Segal M (2014) Dendritic spines: the locus of structural and functional plasticity. Physiol Rev 94:141–188.
Schikorski T, Stevens CF (2001) Morphological correlates of functionally defined synaptic vesicle populations. Nat Neurosci 4:391–395.
Sells MA, Knaus UG, Bagrodia S, Ambrose DM, Bokoch GM, Chernoff J (1997) Human p21-activated kinase (Pak1) regulates actin organization in mammalian cells. Curr Biol 7:202–210.
Shekarabi M, Moore SW, Tritsch NX, Morris SJ, Bouchard JF, Kennedy TE (2005) Deleted in colorectal cancer binding Netrin-1 mediates cell substrate adhesion and recruits Cdc42, Rac1, Pak1, and N-WASP into an intracellular signaling complex that promotes growth cone expansion. J Neurosci 25:3132–3141.
Sheng M, Kim E (2011) The postsynaptic organization of synapses. Cold Spring Harb Perspect Biol 3:a005678.
Sholl DA (1953) Dendritic organization in the neurons of the visual and motor cortices of the cat. J Anat 87:387–406.
Soderling SH, Guire ES, Kaech S, White J, Zhang F, Schutz K, Langeberg LK, Banker G, Raber J, Scott JD (2007) A WAVE-1 and WRP signaling complex regulates spine density, synaptic plasticity, and memory. J Neurosci 27:355–365.
Stein E, Huynh-Do U, Lane AA, Cerretti DP, Daniel TO (1998) Nck recruitment to Eph receptor, EphB1/ELK, couples ligand activation to c-Jun kinase. J Biol Chem 273:1303–1308.
Tada T, Sheng M (2006) Molecular mechanisms of dendritic spine morphogenesis. Curr Opin Neurobiol 16:95–101.
Tashiro A, Yuste R (2004) Regulation of dendritic spine motility and stability by Rac1 and Rho kinase: evidence for two forms of spine motility. Mol Cell Neurosci 26:429–440.
Tashiro A, Minden A, Yuste R (2000) Regulation of dendritic spine morphology by the rho family of small GTPases: antagonistic roles of Rac and Rho. Cereb Cortex 10:927–938.

Tehrani S, Tomasevic N, Weed S, Sakowicz R, Cooper JA (2007) Src phosphorylation of cortactin enhances actin assembly. Proc Natl Acad Sci U S A 104:11933–11938.

Thévenot E, Moreau AW, Rousseau V, Combeau G, Domenichini F, Jacquet C, Goupille O, Amar M, Kreis P, Fossier P, Barnier J-V (2011) p21-activated kinase 3 (PAK3) protein regulates synaptic transmission through its interaction with the Nck2/Grb4 protein adaptor. J Biol Chem 286:40044–40059.

Urbán N, Guillemot F (2014) Neurogenesis in the embryonic and adult brain: same regulators, different roles. Front Cell Neurosci 8:396.

Vilà-Balló A, Mas-Herrero E, Ripollés P, Simó M, Miró J, Cucurell D, López-Barroso D, Juncadella M, Marco-Pallarés J, Falip M, Rodríguez-Fornells A (2017) Unraveling the role of the hippocampus in reversal learning. J Neurosci 37:6686–6697.

Wang L, Conner JM, Rickert J, Tuszynski MH (2011) Structural plasticity within highly specific neuronal populations identifies a unique parcellation of motor learning in the adult brain. Proc Natl Acad Sci U S A 108:2545–2550.

Wegmeyer H, Egea J, Rabe N, Gezelius H, Filosa AE, Varoqueaux F, Deininger K, Schnutgen F, Brose N, Klein R, Kullander K, Betz A (2007) EphA4-dependent axon guidance is mediated by the RacGAP alpha2-chimaerin. Neuron 55:756–767.

Wigerius M, Quinn D, Diab A, Clattenburg L, Kolar A, Qi J, Krueger SR, Fawcett JP (2018) The polarity protein angiomotin p130 controls dendritic spine maturation. J Cell Biol 217:715–730.

Wong AA, Brown RE (2007) Age-related changes in visual acuity, learning and memory in C57BL/6J and DBA/2J mice. Neurobiol Aging 28:1577–1593.

Wong EW, Glasgow SD, Trigiani LJ, Chitsaz D, Rymar V, Sadikot A, Ruthazer ES, Hamel E, Kennedy TE (2019) Spatial memory formation requires netrin-1 expression by neurons in the adult mammalian brain. Learn Mem 26:77–83.

Woolfrey KM, Srivastava DP (2016) Control of dendritic spine morphological and functional plasticity by small GTPases. Neural Plast 2016:3025948.

Xu T, Yu X, Perlik AJ, Tobin WF, Zweig JA, Tennant K, Jones T, Zuo Y (2009) Rapid formation and selective stabilization of synapses for enduring motor memories. Nature 462:915–919.

Yang G, Pan F, Gan W-B (2009) Stably maintained dendritic spines are associated with lifelong memories. Nature 462:920–924.

Zhao Z, Manser E, Lim L (2000) Interaction between PAK and Nck: a template for Nck targets and role of PAK autophosphorylation. Mol Cell Biol 20:3906–3917.